Associated Scientist final report

AC_AVS21_01

AC SAF GOME-2 Level 3 product validation

July 2021 – March 2022

Prepared by: Ka Lok Chan, Rutherford Appleton Laboratory
AC SAF supervisor: Pieter Valks, DLR

AC SAF VALIDATION REPORT

Validated products:

Identifier	Acronym	Name	Satellite(s)
O3M-303	MxG-O-O3-daily	Level 3 daily averaged total ozone	MetopA, MetopB & MetopC
O3M-340	MxG-O-NO2-daily	Level 3 dailly averaged total NO_2	
O3M-343	MxG-O-NO2Tr-daily	Level 3 daily averaged tropospheric NO_2	
O3M-318	MxG-O-BrO-daily	Level 3 daily averaged BrO	
O3M-387	MxG-O-H2O-daily	Level 3 daily averaged H_2O	
O3M-346	MxG-O-HCHO-daily	Level 3 daily averaged HCHO	
O3M-376	MxG-O-SO2-daily	Level 3 daily averaged SO_2	
O3M-388	MxG-O-O3-monthly	Level 3 monthly averaged total ozone	
O3M-389	MxG-O-NO2-monthly	Level 3 monthly averaged total NO_2	
O3M-390	MxG-O-NO2Tr-monthly	Level 3 monthly averaged tropospheric NO_2	
O3M-391	MxG-O-BrO-monthly	Level 3 monthly averaged BrO	
O3M-393	MxG-O-H2O-monthly	Level 3 monthly averaged H2O	
O3M-394	MxG-O-HCHO-monthly	Level 3 monthly averaged HCHO	
O3M-397	MxG-O-SO2-monthly	Level 3 monthly averaged SO_2	

Authors:

Name	Institute
Ka Lok Chan	Rutherford Appleton Laboratory
Pieter Valks	German Aerospace Center

Reporting period:	GOME-2/Metop-A | Jan 2007 - Dec 2020
	GOME-2/Metop-B | Jan 2013 - Dec 2020
	GOME-2/Metop-C | Feb 2019 - Dec 2020

Input data versions:	GOME-2A L2 GDP 4.8 GOME-2B L2 GDP 4.8 GOME-2C L2 GDP 4.9
Data processor versions:	G2_L3_TC v1.0

Introduction to EUMETSAT Satellite Application Facility on Atmospheric Composition monitoring (AC SAF)

Background

The need for atmospheric chemistry monitoring was first realized when severe loss of stratospheric ozone was detected over the Polar Regions. At the same time, increased levels of ultraviolet radiation were observed.

Ultraviolet radiation is known to be dangerous to humans and animals (causing e.g., skin cancer, cataract, immune suppression) and having harmful effects on agriculture, forests and oceanic food chain. In addition, the global warming - besides affecting the atmospheric chemistry - also enhances the ozone depletion by cooling the stratosphere. Combined, these phenomena have immense effects on the whole planet. Therefore, monitoring the chemical composition of the atmosphere is a very important duty for EUMETSAT and the world-wide scientific community.

Objectives

The main objectives of the AC SAF are to process, archive, validate and disseminate atmospheric composition products (O_3, NO_2, SO_2, BrO, HCHO, H_2O and OClO), aerosol products and surface ultraviolet radiation products utilising the satellites of EUMETSAT. The majority of the AC SAF products are based on data from the GOME-2 spectrometers onboard Metop-A and Metop-B satellites.

Another important task of the AC SAF is the research and development in radiative transfer modelling and inversion methods for obtaining long-term, high-quality atmospheric composition products from the satellite measurements.

Product categories, timeliness and dissemination

Data products are divided in two categories depending on how quickly they are available to users:

Near real-time products are available in less than three hours after measurement. These products are disseminated via EUMETCast, WMO GTS or internet.

- Near real-time trace gas columns
  - O_3, NO_2, HCHO, SO_2
- Near real-time ozone profiles
  - coarse and high-resolution
- Near real-time absorbing aerosol indexes
  - from main science channels and polarization measurement detectors
- Near real-time UV indexes
  - clear-sky and cloud-corrected

Offline products are available in two weeks after measurement and disseminated via dedicated web services at EUMETSAT, FMI and DLR.

- Offline trace gas columns
  - O_3, NO_2, SO_2, BrO, HCHO, H_2O and OClO
- Offline ozone profiles
  - coarse and high-resolution
- Offline absorbing aerosol indexes
  - from main science channels and polarization measurement detectors

- Offline surface UV

More information about the AC SAF project, products and services: https://acsaf.org/

AC SAF Helpdesk: helpdesk@acsaf.org

Twitter: https://twitter.com/Atmospheric_SAF

CONTENTS

ACRONYMS AND ABBREVIATIONS

AC SAF	SAF on Atmospheric Chemistry Monitoring
AMF	Air Mass Factor
BRDF	Bidirectional Reflectance Distribution Function
DLR	German Aerospace Centre
DOAS	Differential Optical Absorption Spectroscopy
ECV	Essential Climate Variable
ESA	European Space Agency
EUMETSAT	European Organisation for the Exploitation of Meteorological Satellites
FDCR	Fundamental Climate Data Record
FMI	Finnish Meteorological Institute
GCOS	Global Climate Observing System
GDP	GOME Data Processor
GOME	Global Ozone Monitoring Experiment
H2O	Water Vapour
IMF	Remote Sensing Technology Institute
ITCZ	Intertropical Convergence Zone
LOS	Line Of Sight
NIR	Near-infrared
NO2	Nitrogen Dioxide
REMSS	Remote Sensing System
RMSE	Root Mean Square Error
SAD	Scan Angle Dependency
SCD	Slant Column Density
SSD	Service Specification Document
SSMIS	Special Sensor Microwave Imager Sounder
SZA	Solar Zenith Angle
TCDR	Thematic Climate Data Record
TCWV	Total Column Water Vapour
UPAS	Universal Processor for UV/VIS Atmospheric Spectrometers
VIS	Visible
VCD	Vertical Column Density

Applicable AC SAF Documents

[ATBD_L3daily] Algorithm Theoretical Basis Document for GOME-2 NO_2, H_2O, O_3, SO_2, HCHO and BrO Level 3 daily gridded products, K. L. Chan and P. Valks, SAF/AC/DLR/ATBD/L3daily, 12.01.2021, 2021.

[ATBD_L3monthly] Algorithm Theoretical Basis Document for GOME-2 NO_2, H_2O, O_3, SO_2, HCHO and BrO Level 3 daily gridded products, K. L. Chan and P. Valks, SAF/AC/DLR/ATBD/L3mon, 12.01.2021, 2021.

[PUM] Product User Manual for GOME-2 Total Column Products of Ozone, NO_2, BrO, SO_2, H_2O, HCHO, OCIO and Cloud Properties (GDP 4.9 for AC SAF OTO and NTO), SAF/AC/DLR/PUM/01, 3/B Rev.1, Valks, P., et. al., 2019. https://acsaf.org/docs/pum/Product_User_Manual_NTO_OTO_Nov_2019.pdf last accessed: 15.11.2020.

[PRD] Product Requirements Document, Issue 1.5, SAF/AC/FMI/RQ/PRD/001, Issue 1.5, D. Hovila, S. Hassinen, P. Valks, J., S. Kiemle, O. Tuinder, H. Joench-Soerensen, June 2019.

Acknowledgments

Part of the results presented in this work have been produced using the Aristotle University of Thessaloniki High Performance Computing Infrastructure and Resources. M.E.K. would like to acknowledge the support provided by the IT Center of the Aristotle University of Thessaloniki throughout the progress of this research work. M.E.K. further acknowledges the support by the Atmospheric Toolbox®.

1. INTRODUCTION AND OBJECTIVES

Satellite remote sensing observations provide indispensable spatio-temporal information of atmospheric composition on a global scale. However, these satellite data are usually provided at the instrument resolution which is expressed in the satellite viewing geometry of reference using across-track and along-track position. In addition, these data are not in regular latitude-longitude grid and often multiple pixels overlapping at the edges of orbit within a day. Using this kind of scientific product requires very good knowledge of the satellite product, especially when averaging multiple measurements to generate daily or monthly maps. The GOME-2 level 3 products are user-friendly satellite products by re-projecting and averaging the GOME-2 level 2 data onto a regular longitude–latitude grid. The purpose of this document is to present the validation/verification of the GOME-2 Level 3 daily and monthly gridded products. These products contain global daily and monthly mean ozone (O_3), total and tropospheric nitrogen dioxide (NO_2), bromine oxide (BrO), water vapour (H_2O), formaldehyde (HCHO), and sulphur dioxide (SO2).

As the GOME-2 level 3 products are generated from the level 2 datasets which have already been fully validated. Therefore, the focus of this study is to investigate the consistency of level 2 and 3 products. In addition, the spatial sampling resolution of the level 3 product is also an important issue. To verify and validate GOME-2 level 3 products this study focuses on the following aspects:

1) To investigate the spatial resolution of level 3 products still preserve the original spatial features captured in the level 2 data
2) To verify the consistency between level 2 and 3 products
3) To examine the consistency among the three GOME-2 sensors
4) To validate the level 3 products by comparing to ground-based observations

2. OBSERVATIONAL DATASETS

2.1 GOME-2 on MetopA, MetopB & MetopC Level-3 Data

The GOME-2 sensor (Munro et al., 2016) is a nadir viewing scanning spectrometer which covers the spectral range from 240 to 790 nm, with a spectral resolution of about 0.54 nm in the visible spectral region. Additionally, two polarization components are measured with polarization measurement devices (PMDs) using 30 broadband channels covering the full spectral range at higher spatial resolution. The German Aerospace Centre (DLR) plays a major role in the design, implementation and operation of the GOME-2 ground segment for trace gas products, as well as cloud properties in the framework of the EUMETSAT's AC SAF project.

The first GOME-2 instrument was mounted on the Metop-A satellite (GOME-2A), which followed a sun-synchronous orbit with a mean altitude of 817 km. The overpass local time at the equator was 09:30 Local Time (LT) with a repeat cycle of 29 days. Metop-A was launched on the 19th of October 2006 and operational GOME-2 products are available from January 2007 until November 2021. A second GOME-2 type sensor on board of the Metop-B satellite (GOME-2B) was launched on the 17th of September 2012 and has been fully operational since December 2012. GOME-2 tandem operations started on 15 July 2013. In the tandem mode, GOME-2A operated on a reduced swath width of 960 km, thereby increasing its spatial resolution (40 by 40 km), while GOME-2B continues to operate on a nominal wide swath of 1920 km. This configuration allowed the use of the higher spatial resolution data to further study the consistency of the two products in the overlap regions of the GOME-2A and GOME-2B orbits. Finally, the third satellite of the EUMETSAT Polar System series, GOME-2/Metop-C, was launched on the 7th of November 2018 and provides operational data since January 2019. The main characteristics of the three GOME-2 instruments are summarized in Table 1.

Table 1. Summary of the GOME-2 instrument characteristics.

Sensor Satellite	**GOME-2 Metop-A**	**GOME-2 Metop-B**	**GOME-2 Metop-C**
Data period	01/2007 – 11/2021	12/2012 - present	01/2019 - present
Spectral coverage	240 - 790 nm	240 - 790 nm	240 - 790 nm
Ground pixel size	80 x 40 km^2 – 40 x 40 km^2 (*)	80 x 40 km^2	80 x 40 km^2
Swath width	1920 km - 960 km (*)	1920 km	1920 km
Equator crossing time	9:30 a.m. LT	9:30 a.m. LT	9:30 a.m. LT
Global coverage	1.5 days	1.5 days	1.5 days

(*) GOME-2A tandem operation since 15 July 2013.

The creation of GOME-2 L3 daily and monthly data is described in detail in [ATBD_L3daily] and [ATBD_L3monthly]. In summary, a latitude-longitude grid of 0.25º×0.25º was used for translating the spatial information expressed in the GOME-2 ground pixels into a regular latitude longitude grid

system. The binning process for the data set included taking the arithmetic mean and standard deviation of all L2 data points falling into the grid cell in a given day or month respectively using only forward-scan pixels. Because of the relatively large GOME-2 pixel size, a significant grid effect would be induced by assigning each GOME-2 measurement to a single grid point based on the center coordinates of the GOME-2 ground pixel, without taking into account the pixel geometry and extension. Therefore, the re-gridding process considers the overlapping area of GOME-2 ground pixel and latitude longitude grid. For a grid cell partially overlapped with the satellite pixel, the percentage of overlap is calculated and used as weighting for the calculation of mean value. When a satellite pixel fully covers the entire grid cell it is considered as 100% overlap.

The GOME-2 level 3 products are in two different temporal resolution, daily and monthly. Both daily and monthly level 3 product consists of gridded trace gas columns and other auxiliary parameters, i.e., cloud, surface and statistical parameters. The level 3 products are separated for each species (i.e., O_3, NO_2, water vapour, BrO, HCHO and SO_2) and each GOME-2 instrument (i.e., GOME-2A, B and C). All products are in a spatial resolution of 0.25° × 0.25° with coordinates range from 180° W to 180° E in longitude and from 90° S to 90° N in latitude (720 (latitude) × 1440 (longitude) grid cell). Figure 1 shows an example of the daily level 3 product for all trace gases and all GOME-2 instruments, while example of monthly level 3 data is shown in Figure 2.

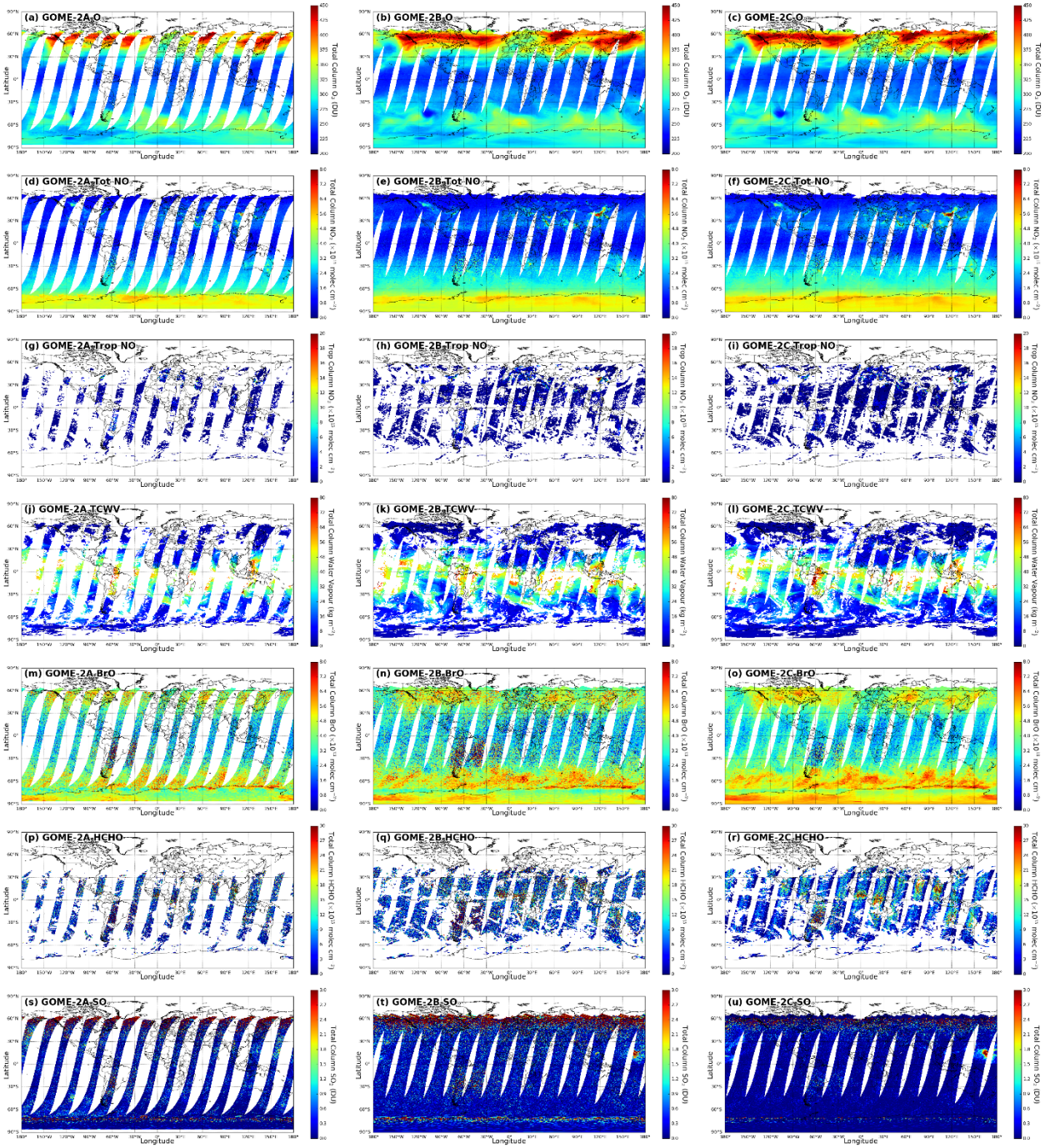

Figure 1. Daily level 3 product of GOME-2A (1st column), GOME-2B (2nd column), and GOME-2C (3th column) for 15 January 2020. Total column O_3 (1st row), total column NO_2 (2nd row), tropospheric column NO_2 (3th row), total column water vapour (4th row), total column BrO (5th row), total column HCHO (6th row), and total column SO_2 (7th row) are shown.

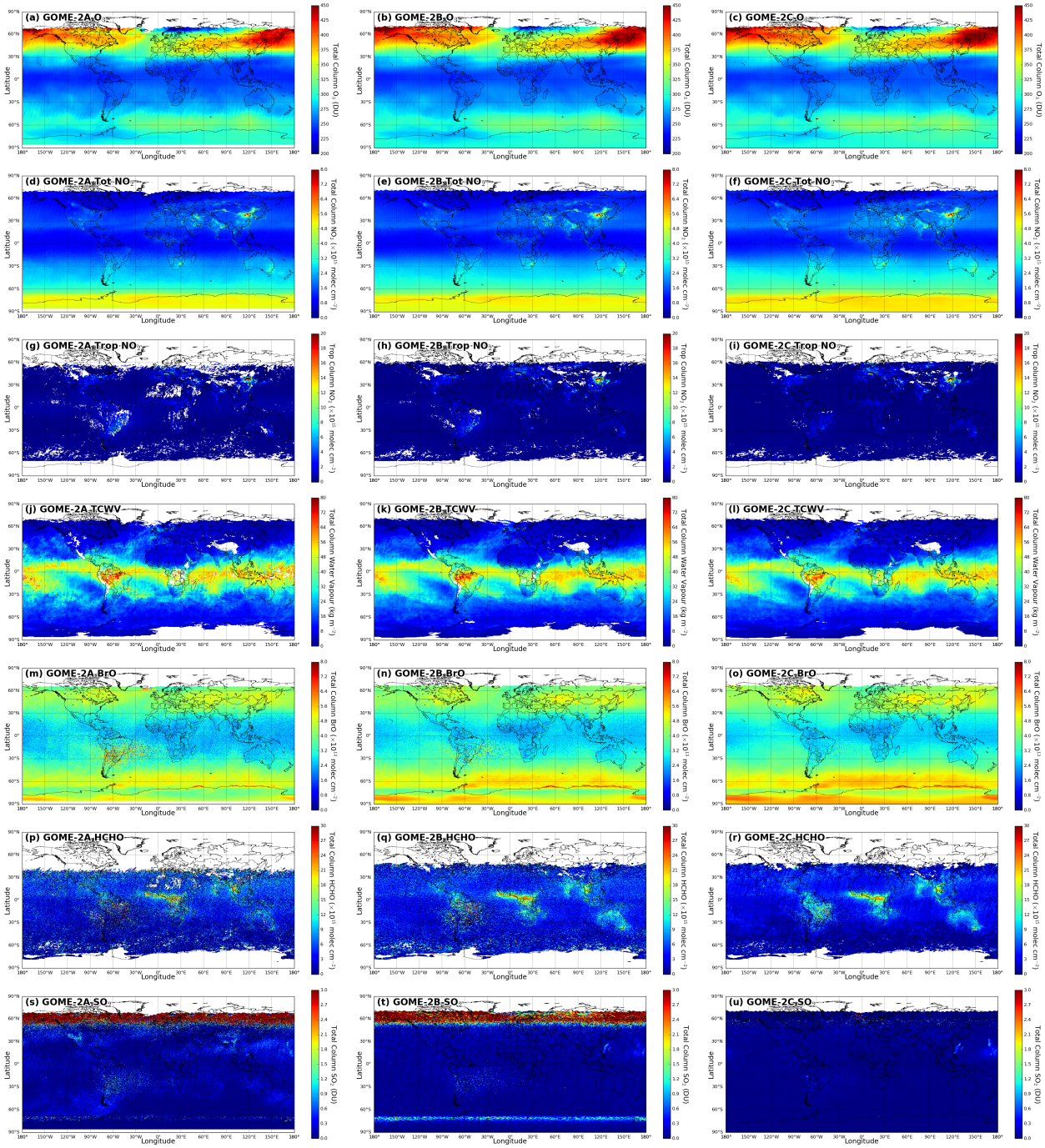

Figure 2. Monthly level 3 product of GOME-2A (1st column), GOME-2B (2nd column), and GOME-2C (3th column) for January 2020. Total column O_3 (1st row), total column NO_2 (2nd row), tropospheric column NO_2 (3th row), total column water vapour (4th row), total column BrO (5th row), total column HCHO (6th row), and total column SO_2 (7th row) are shown.

2.2 Brewer Ozone Observations

The Brewer data are obtained the World Ozone and Ultraviolet Radiation Data Centre (WOUDC, http://www.woudc.org). The WOUDC data centre is part of the Global Atmosphere Watch (GAW) programme of the World Meteorological Organization (WMO), providing quality-assured Brewer

and Dobson measurements. Brewer and Dobson instruments measure intensity at several wavelength channel in the UV band. The Brewer data has long been used to validate satellite observations of ozone (Balis et al., 2007a, b; Antón et al., 2009; Loyola et al., 2011; Koukouli et al., 2012, 2015; Garane et al., 2018, 2019). In this study, we only use the direct sun Brewer observations of total column O_3 for the validation of GOME-2 Level 3 product.

2.3 ZSL-DOAS and MAX-DOAS NO_2 Observations

Zenith-Scattered-Light Differential Optical Absorption Spectroscopy (ZSL-DOAS) data are obtained from the framework of the Network for the Detection of Atmospheric Composition Change (NDACC). NDACC ZSL-DOAS network provides total column NO_2 observations with standardized operating procedures and harmonized retrieval methods. ZSL-DOAS data from NDACC stations is available on the NDACC Data Host Facility (see http://www.ndacc.org). ZSL-DOAS measurements during twilight periods are sensitive to stratospheric absorbers due to the geometrical enhancement of the optical path in the stratosphere. Therefore, it has long been used for the validation of satellite total NO_2 observations (Ionov et al. 2008, Celarier et al. 2008). The retrieval of total column NO_2 from ZSL-DOAS observations based on the Langley method, which calculate the corresponding air mass factor according to its observation and solar geometry. In this study, ZSL-DOAS observations of total column NO_2 during the morning twilight period are used to validate GOME-2 Level 3 total NO_2 products.

The Multi-AXis Differential Optical Absorption Spectroscopy (MAX-DOAS) is a passive remote sensing technique which uses spectroscopic observations of scattered sunlight with different viewing zenith angles to derive column densities of trace gas. Due to its compact experimental setup and sensitivity to lower troposphere, it has been widely used for the validation of satellite observations of tropospheric column NO_2 (Brinksma et al. 2008; Celarier et al. 2008; Irie et al. 2008; Ma et al. 2013; Kanaya et al. 2014; Takashima et al. 2015; Drosoglou et al. 2017; Chan et al., 2018, 2019, 2020; Compernolle et al. 2020). The ground-based MAX-DOAS instruments are operated by various research institutes around the world, and the data is centrally managed by BIRA-IASB within the framework of the S5PVT AO project NIDFORVAL (S5P NItrogen Dioxide and FORmaldehyde Validation using NDACC and complementary FTIR and UV-Vis DOAS ground-based remote sensing data). The affiliation of MAX-DOAS instruments in the NDACC network is still under progress, following efforts done in the NORS, QA4ECV and ESA's FRM4DOAS project to harmonize and automatize data processing. In this study, MAX-DOAS observations tropospheric column NO_2 are used to validate GOME-2 Level 3 tropospheric NO_2 products.

2.4 Sun-photometer Water Vapour Observations

The CIMEL CE-318 sun-photometers are used in the AERosol RObotic NETwork (AERONET) to measure direct sun and sky radiance at multiple wavelengths (Holben et al., 1998). These sun-photometer observations do not only provide information of aerosol optical properties (Holben et al., 2001) but also of columnar water vapour content (Alexandrov et al., 2009). Water vapour columns are retrieved from sun-photometer observations in the near infrared (NIR) at 940 nm where water vapor absorption is rather strong. The inversion of water vapor columns is based on the attenuation of radiation through the atmosphere. A more detailed description of the water vapor retrieval algorithm can be found in Alexandrov et al. (2009). In total, there are over 1000 AERONET stations around the globe providing columnar water vapor observations. The AERONET water vapour

product has also been validated by microwave radiometry, GPS and radiosondes measurements (Pérez-Ramírez et al., 2014). The sun-photometer measurements are in general underestimating the columnar water vapour by 6 - 9 % (Pérez-Ramírez et al., 2014). In this study, cloud screened, and quality assured level 2.0 data are used to validate the GOME-2 Level 3 total column water vapour products.

2.5 MAX-DOAS HCHO Observations

Ground-based MAX-DOAS observations are used to validate GOME-2 Level 3 total column HCHO products. MAX-DOAS observation of HCHO has long been used for satellite validation (Vigouroux et al. 2009; Li et al. 2013; Chan et al. 2019, 2020; Kumar et al. 2020, De Smedt et al. 2021). The retrieval of HCHO columns from MAX-DOAS observations are performed within a wavelength range similar to the GOME-2 retrieval, i.e., 328-359nm. The ground-based MAX-DOAS instruments are operated by various research institutes around the world, and the data is centrally managed by BIRA-IASB.

2.6 ZSL-DOAS BrO Observations

Sea ice is a significant source of BrO which causes ozone depletion in Polar Regions. Therefore, the ZSL-DOAS observations at Harestua (60.22°N, 10.75°E), Norway are used to validate the GOME-2 Level 3 total column BrO product. The operation of the ZSL-DOAS instrument and the retrieval of BrO column are performed by IASB-BIRA. Detailed description of the ZSL-DOAS instrument setup and BrO column retrieval algorithm can be found in Hendrick et al., 2007.

2.7 Pandora SO_2 Observations

The Pandonia Global Network is a direct-sun spectrometer network used to monitor trace gas values worldwide. The Pandora spectrometer instrument spectroscopy is used to measure columnar amounts of trace gases in the atmosphere. Pandora determines trace gas amounts from direct sun observations by using the DOAS technique with theoretical solar spectrum as a reference. As the anthropogenic SO_2 emission has been reduced significantly in the recent decades, the background SO_2 level is mostly zero around the globe and only few locations with signification anthropogenic SO_2 source. Considering the low background SO_2 level and the large measurement noise of SO_2 data, it is more appropriate to validate the satellite observations over location with significant variation and sources. Mexico City is one of the few places with significant anthropogenic SO_2 sources. Therefore, we use the Pandora SO_2 observations at Mexico City to validate GOME-2 Level 3 total column SO_2 products.

2.8 Verification and Validation Methodology

To investigate whether the selection of the spatial resolution of the regular latitude-longitude grid of the level 3 products is appropriate, we are regidding the level 2 product onto different resolution and compare to the original level 2 data. This process will also provide information on the consistency between level 2 and 3 products.

To examine the consistency among the three GOME-2 sensors, we are looking into the time series of global averages and bias among the three GOME-2 sensors. In addition, we are also looking into the time series of zonal pattern of each product to investigate the zonal consistency.

To verify and validate the absolute value of each GOME-2 level 3 product, we compare the GOME-2 observations to co-located ground-based measurements. Total ozone product is compared to Brewer observations, total NO_2 product is compared to ZSL-DOAS, and tropospheric NO_2 product is compared to MAX-DOAS observations. Total column water vapour product is compared to sun-photometer data, total HCHO product is compared to MAX-DOAS observations, total BrO product is compared to ZSL-DOAS observations in Norway, and total SO_2 product is compared to Pandora direct sun spectrometer measurement in Mexico.

The following criteria are applied to co-locate the GOME-2 products and ground-based reference data sets.

1) The grid cell of the Level 3 GOME-2 products covering the ground-based measurement site is paired with the daily/monthly ground-based measurements
2) For ground-based Brewer, MAX-DOAS, sun-photometer and Pandora data, they are temporally averaged around the GOME-2 overpass time from 8:30 to 10:30
3) For ZSL-DOAS measurements, the average of morning twilight period is used

After co-locating the GOME-2 and ground-based datasets, we compare the GOME-2 and ground-based data sets through scatter plot, histogram of the differences, and sort the differences/bias by year, latitude band or measurement site as box plot and time series.

3. RESULTS

3.1 Sampling resolution

The processing of GOME-2 level 3 data requires binning of the level 2 data which is onto a regular 2-dimensional latitude-longitude grid. The selection of the resolution of the regular latitude-longitude grid is important. On one hand, it is important to preserve the original spatial features captured in the level 2 data with higher spatial resolution, but on the other hand, it is necessary to keep the data files in a reasonable size and keep it user friendly.

To select the best spatial resolution for the level 3 product, we have analysed the results with various resolutions, i.e., 0.1° × 0.1°, 0.25° × 0.25° and 0.5° × 0.5°. Figure 3 shows GOME-2A data of each trace gas species gridded in different resolutions and level 2 data in the original instrument resolution for an orbit over North China on 15 July 2014. Missing data are mainly due to filtering of cloudy pixels and other low-quality observations. GOME-2A data is shown due to its highest spatial resolution among all three GOME-2 instruments (GOME-2A: 40 km × 40 km, GOME-2B&C: 40 km × 80 km). We looked into the spatial smoothing/averaging effect over North China, as this region is expected to show some strong spatial gradient of tropospheric pollutants, i.e., NO_2. Missing data are mainly due to cloudiness. Data in all four resolutions show very similar spatial structures. The absolute values of the level 3 data are also consistence with the level 2 product. The results show gridding GOME-2 data with higher spatial resolution (i.e., 0.1°) better preserve the original GOME-2 instrument footprint. However, lower resolution of 0.25° can also preserve the spatial pattern of fast varying tropospheric species, i.e., NO_2. While a rather strong smoothing/averaging effect is observed from data gridded with lower spatial resolution (i.e., 0.5°).

Figure 4 shows monthly averaged GOME-2A data of each trace gas species gridded in different resolutions over North China in July 2014. Difference between data gridded with different resolutions are also shown for reference. Data gridded in all three resolutions show very similar spatial structures. Hotspots of anthropogenic pollutants, i.e., tropospheric NO_2, can be clearly observed from the monthly averaged data. Species with major contribution from natural sources, e.g., O_3 and water vapour, show rather smooth appearance. Despite large numbers of observations are included in the monthly averaging process, species with lower signal to noise ratio, e.g., HCHO and SO_2, still show rather high background noise. This is mainly due to the low signal to noise ratio of these species. This effect is as expected more significant for data gridded in higher spatial resolution, i.e., 0.1°, due to less spatial averaging. Traces of the satellite footprints can still be seen in the 0.1° resolution monthly averaged data, while the satellite footprints are much less significant in the 0.25° and 0.5° resolution data. The differential plots between data gridded with 0.1° and 0.25° resolution in general show only small differences. Slightly larger discrepancies mainly appear over pollution hotspots, i.e., for tropospheric NO_2. In contrast, data in 0.5° resolution show much bigger differences from 0.1° resolution data. Compared to 0.25° resolution data, 0.1° resolution data shows 2 to 4 times higher underestimation of tropospheric column NO_2 over pollution hotspots. The comparison of GOME-2 data gridded in different resolutions indicates that 0.25° resolution is a balance to preserve the satellite resolution (GOME-2A: 40 km × 40 km, GOME-2B&C: 40 km × 80 km) while capturing the strong spatial variations in most of the tropospheric gases, i.e., NO_2, water vapour and HCHO. In addition, the data size of level 3 products with 0.1° × 0.1° resolution is about 6 times larger than that of 0.25° × 0.25°, while the information content does not show significant difference, especially for monthly products. Therefore, we concluded that 0.25° × 0.25° resolution is a suitable choice for GOME-2 level 3 products.

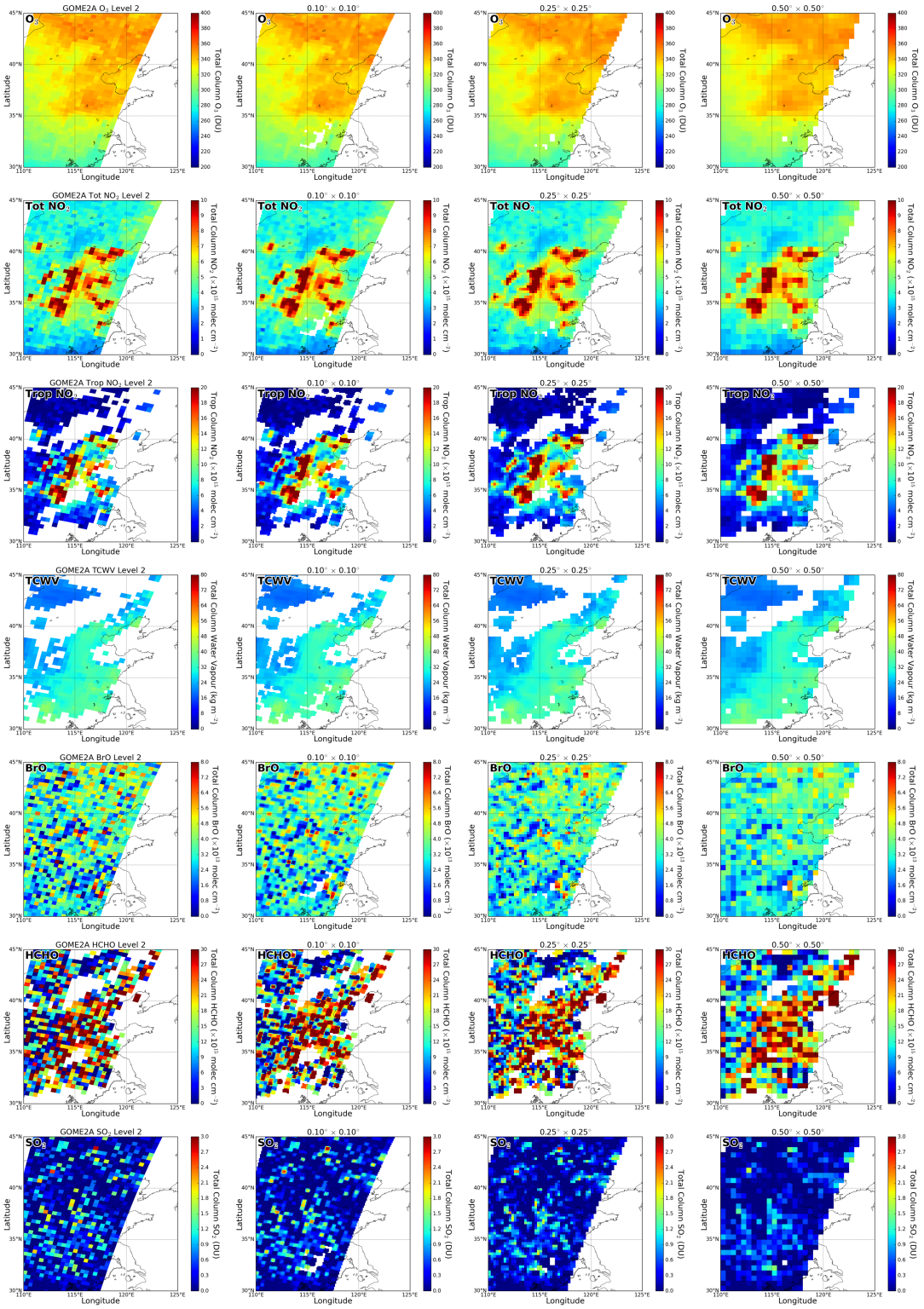

Figure 3. GOME-2A observations of total column O_3 (1st row), total column NO_2 (2nd row), tropospheric column NO_2 (3th row), total column water vapour (4th row), total column BrO (5th row), total column HCHO (6th row), and total column SO_2 (7th row). Data are shown in the original instrument resolution (1st column from the left), gridded with 0.1° × 0.1° resolution (2nd column from the left), 0.25° × 0.25° resolution (3th column from the left), and 0.5° × 0.5° resolution (column on the right). GOME-2A observations on 15 July 2014 over North China are shown. Missing data are mainly due to cloudiness.

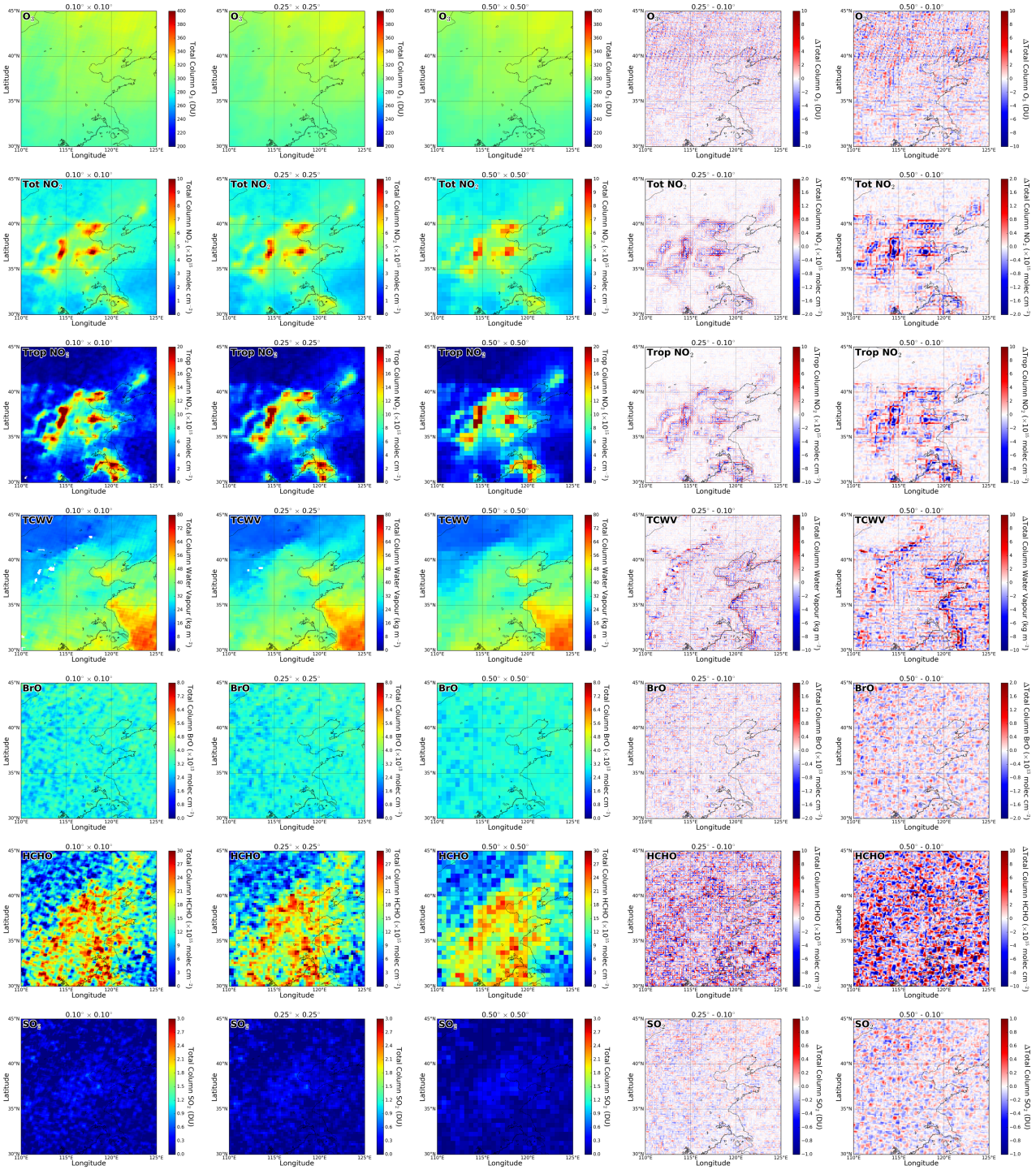

Figure 4. Monthly averaged GOME-2A observations of total column O_3 (1st row), total column NO_2 (2nd row), tropospheric column NO_2 (3th row), total column water (4th row), vapour total column BrO (5th row), total column HCHO (6th row), and total column SO_2 (7th row) over North China in July 2014. Gridded data with 0.1° × 0.1° resolution (1st column from the left), 0.25° × 0.25° resolution (2nd column from the left), and 0.5° × 0.5° resolution (3th column from the left) are shown. Differences between 0.1°, 0.25° and 0.5° are also shown for reference.

3.2 Cross-sensors consistency

3.2.1 Average and bias

Figure 5 shows the global monthly mean time series of (a) total column O_3, (b) total column NO_2, (c) tropospheric column NO_2, (d) total column water vapour, (e) total column BrO, (f) total column HCHO and (g) total column SO_2 for GOME-2A, B & C. The error bars represent the 1σ standard deviation variation. All species show pronounced seasonal variation patterns. The seasonal patterns are related to the natural variability and the variation of coverage area of the GOME-2 measurements.

The global monthly mean O_3 time series of GOME-2A, B & C mostly overlapping with each other, indicating the good agreement among the three sensors.

For total column NO_2, observations from GOME-2A & B show very good consistency, while GOME-2C total column NO_2 are about 1.2×10^{14} molec cm^{-2} higher than that of GOME-2A & B. The tropospheric column NO_2 from GOME-2A & B are also in good agreement. However, GOME-2C observations are about 1.5×10^{14} molec cm^{-2} lower than GOME-2A & B observations. The reason for the biases for GOME-2C total NO_2 columns is related to the GOME-2C instrumental issues which affects GOME-2C spectra for wavelengths < 430 nm. NO_2 DOAS-fit analysis by DLR, BIRA and the Univ. of Bremen during the MetOp-C Commissioning Phase show a large (~30%) positive offset between the NO_2 slant columns from GOME-2C and GOME-2A & B using the standard 425-450 nm fitting window (EUMETSAT, 2019). Therefore, an alternative fitting-window 430.2-465 nm is used for GOME-2C (GDP 4.9). By shifting the fitting range to longer wavelengths for GOME-2C to 430.2 465 nm which includes NO_2 absorption structures between 450 and 465nm, the bias in the NO_2 slant columns between GOME-2C and GOME-2A & B is significantly reduced, while maintaining a high signal-to-noise. Previous validation study shows that the NO_2 slant columns retrieved from GOME-2C observations are slightly higher than that of GOME-2B (Pinardi et al., 2019), indicating the impact of the different spectral fitting bands on the NO_2 retrieval. In addition, the positive bias in the GOME-2C total column NO_2 shows an impact on the tropospheric columns in the stratospheric and tropospheric separation process (Pinardi et al., 2019). Therefore, GOME-2C observations of tropospheric NO_2 column also show a bias of about -15×10^{13} molec cm^{-2} compared to GOME-2A & B, while GOME-2A & B show very good consistency with bias $<1 \times 10^{13}$ molec cm^{-2}.

Total column water vapour measurements from all three GOME-2 sensors also show very consistency with bias smaller than 1 kg m^{-2}.

For BrO observations, GOME-2B measurements show a negative bias of $\sim 1.0 - 1.5 \times 10^{12}$ molec cm^{-2} compared to GOME-2A & C. The discrepancies are partly related to the difference in the scanning swath width and the scan angle dependency (Merlaud et al., 2020). The impact of scan angle dependency on BrO measurements is more significant for GOME-2C compared to GOME-2B, which is likely linked to the polarization sensitivity of the GOME-2C instrument (Merlaud et al., 2020).

GOME-2A observations of total column HCHO are in general $1.5 - 1.9 \times 10^{15}$ molec cm^{-2} lower than GOME-2B & C measurements. Lower HCHO columns are observed by GOME-2A over Amazon, Central Africa, Southeast Asia, and Australia (see Figure 2), thus results slightly lower global averages. Similar to BrO measurements, the scan angle dependency issue is also reported to be significant for GOME-2C HCHO observations (Pinardi et al., 2020). The scan angle dependency effect can also be seen in the BrO and HCHO daily level 3 product.

Total column SO_2 observations from GOME-2C are in general 0.5 DU lower than GOME-2A & B, resulting a slightly negative global average. Higher global average of SO_2 observed by GOME-2A & B is related to the extreme values taken with high solar zenith angle thus low signal to noise ratio (see

Figure 1 & 2), while this effect is much less significant for GOME-2C due to younger instrument age. The overall bias and root mean square of error among the GOME-2 sensors for each product are summarized in Table 1.

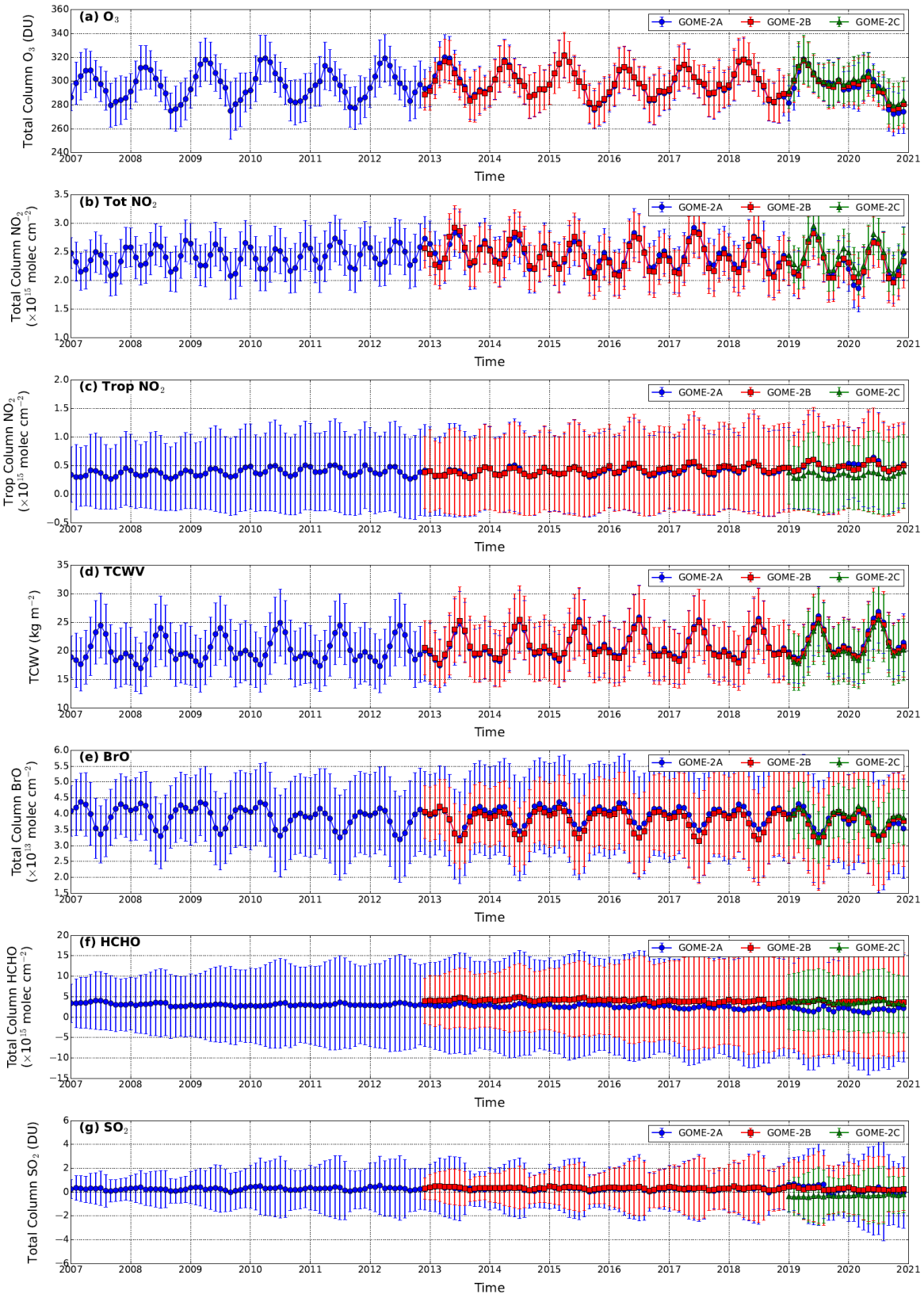

Figure 5. Time series of global monthly mean (a) total column O_3, (b) total column NO_2, (c) tropospheric column NO_2, (d) total column water vapour, (e) total column BrO, (f) total column HCHO and (g) total column SO_2 for GOME-2A

(blue lines), GOME-2B (red lines) and GOME-2C (green lines). The error bars represent the 1σ standard deviation variation.

Table 1. Bias and root mean square error of trace gas columns among the three GOME-2 sensors.

Species (unit)	GOME-2B - GOME-2A[a]		GOME-2C - GOME-2A[b]		GOME-2C - GOME-2B[b]	
	Bias	RMSE	Bias	RMSE	Bias	RMSE
Total O_3 (DU)	0.22 ± 2.24	5.13 ± 1.52	3.36 ± 3.68	7.41 ± 2.52	2.29 ± 0.81	4.60 ± 1.00
Total NO_2 ($\times 10^{13}$ molec cm^{-2})	-2.35 ± 6.31	14.54 ± 2.17	12.05 ± 7.56	18.91 ± 5.79	12.70 ± 3.84	16.33 ± 2.83
Tropo NO_2 ($\times 10^{13}$ molec cm^{-2})	0.69 ± 2.94	63.38 ± 23.37	-15.96 ± 4.93	77.22 ± 11.92	-14.86 ± 3.59	67.05 ± 38.71
TCWV (kg m^{-2})	-0.14 ± 0.36	3.15 ± 0.34	-0.93 ± 0.22	3.35 ± 0.42	-0.52 ± 0.09	2.32 ± 0.30
Total BrO ($\times 10^{12}$ molec cm^{-2})	-1.41 ± 1.25	5.34 ± 1.03	0.52 ± 1.45	6.22 ± 0.59	1.02 ± 0.40	3.37 ± 0.30
Total HCHO ($\times 10^{15}$ molec cm^{-2})	1.54 ± 0.41	8.24 ± 2.19	1.89 ± 0.54	11.00 ± 2.11	-0.08 ± 0.28	5.68 ± 0.55
Total SO_2 (DU)	0.06 ± 0.13	1.21 ± 0.46	-0.53 ± 0.34	2.20 ± 0.51	-0.56 ± 0.14	2.08 ± 0.51

[a] for period from 2013 to 2020

[b] for period from 2019 to 2020

3.2.2 Zonal average

Each GOME-2 monthly averaged level 3 product derived from all three sensors is sorted by latitude and plotted in Figure 6. All three GOME-2 sensors show consistent zonal and seasonal O_3 patterns. Higher O_3 columns are observed over high latitudes, and lower values are found over the tropics. Total column O_3 over the Arctic shows a peak in February to March and a minimum in August to October, while Antarctica displays a reverted seasonal pattern.

Both total and tropospheric column NO_2 from all three GOME-2 sensors show good zonal and seasonal consistency. Elevated total column NO_2 are observed in the Polar Regions during the warm months. This seasonal pattern is attributed to the stratospheric variation of NO_2. Compared to total column NO_2, tropospheric column NO_2 shows a very different zonal and seasonal pattern. Tropospheric NO_2 is mostly concentrated at the mid-latitudes of the northern hemisphere. It is because most of the population are living in this part of the world. Tropospheric NO_2 at mid-latitudes also shows a seasonal pattern with higher values over winter, which is related to higher energy consumption and longer atmospheric lifetime of NO_2 during the cold months. A significant increasing trend of tropospheric NO_2 can be observed by GOME-2A & B over the sub-tropics and mid-latitudes of the southern hemisphere in the recent years (see Figure 6g & h). GOME-2C observed a much less significant enhancement of tropospheric NO_2 in the southern hemisphere, which leads to lower global average tropospheric NO_2 measured by GOME-2C. This discrepancy is likely related to the difference in retrieval wavelength and the subsequent stratosphere and troposphere separation process.

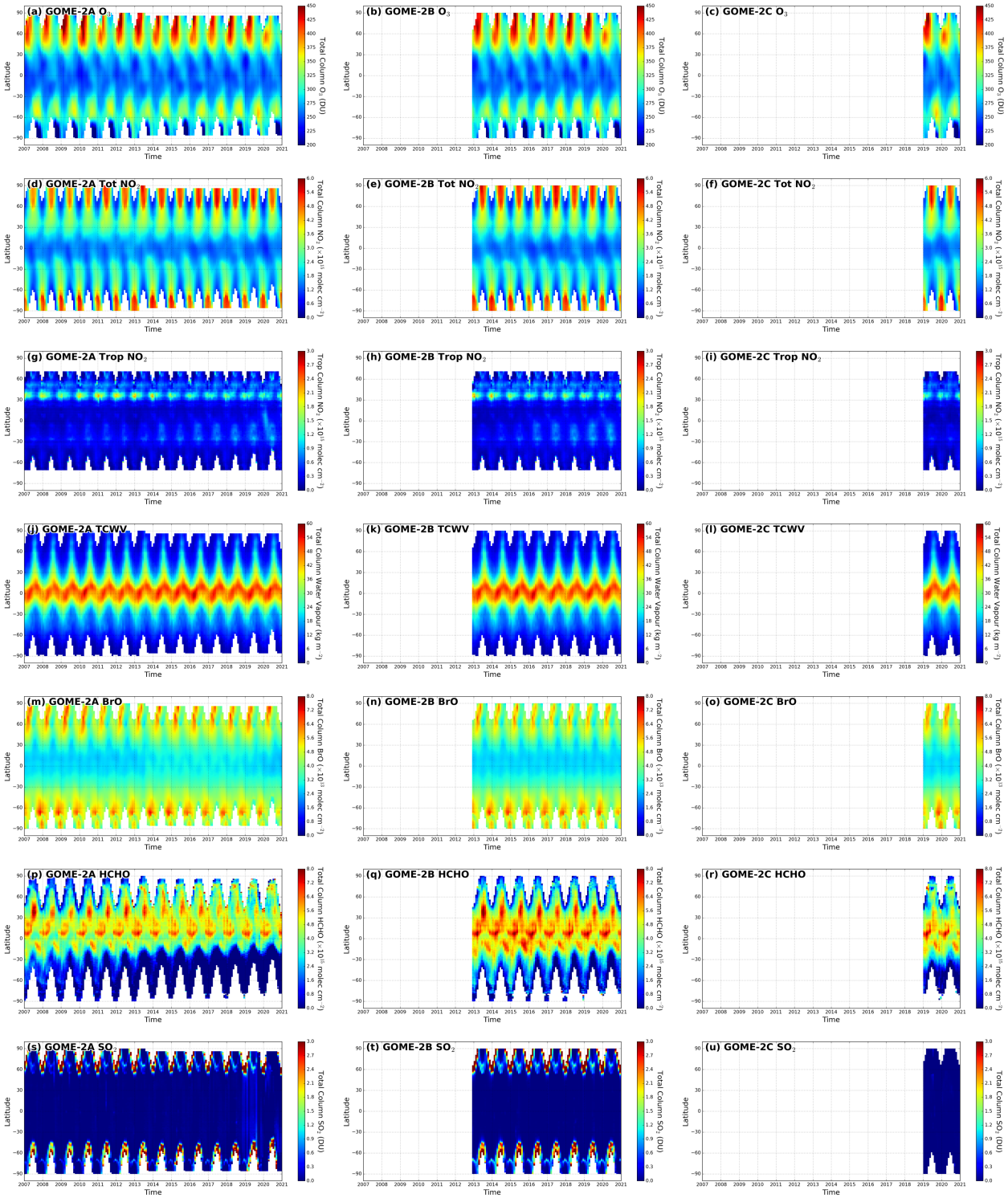

Figure 6. Monthly zonal average of total column O_3 (1st row), total column NO_2 (2nd row), tropospheric column NO_2 (3th row), total column water vapour (4th row), total column BrO (5th row), (total column HCHO (6th row) and total column SO_2 (7th row). Data from GOME-2A (1st column from the left), GOME-2B (2nd column from the left) and (3th column from the left) are shown.

Total column water vapour observations from all three GOME-2 sensors show consistence zonal and seasonal patterns, with higher values in the tropic and lower at high latitudes. Total column water vapour is also higher during the warm months of the corresponding hemisphere.

All three GOME-2 sensors also show very similar zonal and seasonal patterns of total column BrO. However, GOME-2A total column BrO observations from 2014 to 2019 are slightly higher than that of GOME-2B at all latitude band and results a small bias of 1.41×10^{12} molec cm^{-2}. However, when we look into the data from 2020 to 2021, the bias is smaller and result a smaller bias of 0.52×10^{12} molec cm^{-2} with GOME-2C observations.

Total column HCHO from all three GOME-2 sensors show higher values over tropics and sub-tropics, while lower values appear at higher latitudes. Both GOME-2A & B measurements show a significant decreasing trend of HCHO in the southern hemisphere. However, GOME-2A measurements are significantly lower than GOME-2B &C, resulting a bias of -1.54 and -1.89×10^{15} molec cm^{-2} when compared to GOME-2B and GOME-2C observations. The discrepancy is related to the underestimation over HCHO rich regions, e.g., Amazon, Southeast Asia and Australia.

Total SO_2 observations from all three GOME-2 sensors show very low SO_2 levels (very close to 0) around the globe as expected. However, GOME-2A & B measurements show significantly higher noise for measurement with high solar zenith angle, while this effect are much less significant for GOME-2C. Therefore, GOME-2C observations are in general about 0.5 DU lower than GOME-2A & B.

3.3 Ground-based observation comparison

3.3.1 Total column ozone

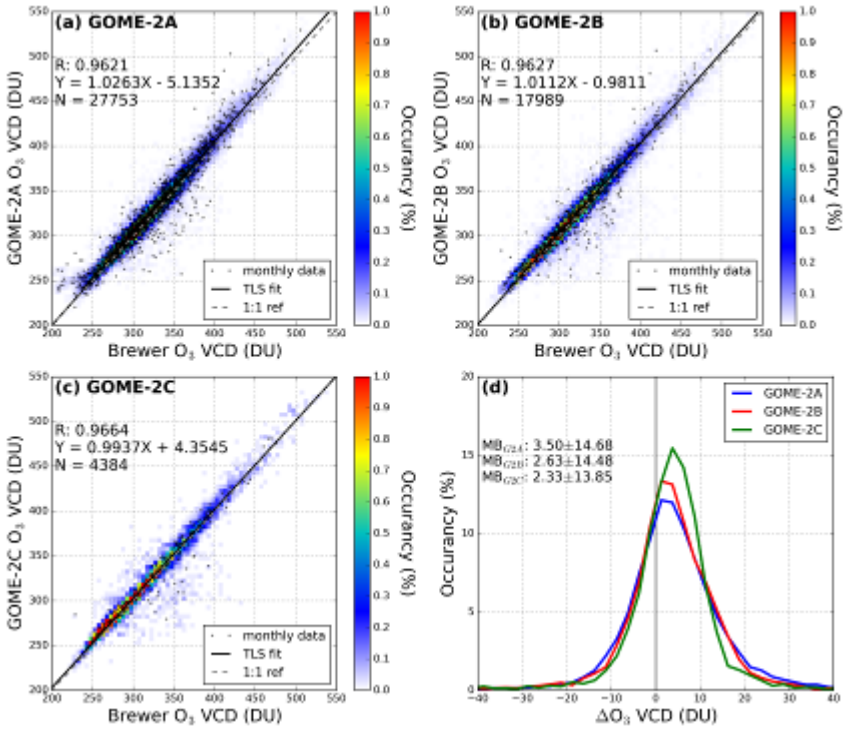

Figure 7. Comparison of daily and monthly total column O_3 measured by the ground-based Brewer instruments to (a) GOME-2A, (b) GOME-2B and (c) GOME-2C. Histograms of the difference of total column O_3 between GOME-2 and Brewer observations are shown in (d).

Daily and monthly GOME-2 level 3 total column ozone are compared to the co-located Brewer observations. Figure 7 shows the density scatter plots for the comparison of total column ozone between GOME-2 and ground-based Brewer observations. Comparisons of GOME-2A, B & C data are shown in Figure 7a, b & c, respectively. Monthly data are also shown. Histograms of the differences between GOME-2 and Brewer observations are shown in Figure 7d. Scatter plots show that GOME-2 monthly data is well in line with the daily data. And the agreement between GOME-2 and Brewer is in general very good with Pearson correlation coefficient (R) of 0.96 for all three GOME-2 sensors. The slopes of the total least squares fit for the comparisons of all three instruments are very close to 1 (1.03 for GOME-2A, 1.01 for GOME-2B, and 0.99 for GOME-2C). The offsets of the total least squares fit range between -5.1 to 4.3 DU. In general, the GOME-2 data sets show a small positive bias of 2.3 to 3.5 DU compared to Brewer observations with standard deviation of 13.9 to 14.7 DU. The bias between all three GOME-2 sensors and ground-based Brewer observations is below 1% which is within the uncertainty of Brewer measurements (Kerr et al. 1988) and fulfils the product requirements.

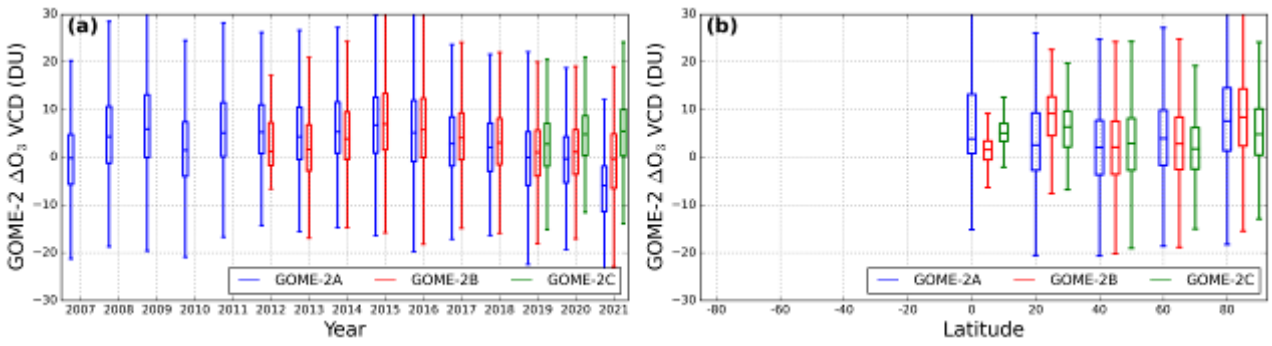

Figure 8. Comparison of total column O_3 between ground-based Brewer instruments and GOME-2 observations. Data are sorted by year in (a), and measurement latitude in (b).

Figure 8 shows box plots of the statistic of the differences of total column ozone between GOME-2 level 3 product and co-located Brewer measurements. GOME-2 data is sorted by the measurement year (Figure 8a) and latitude band (Figure 8b). The box plot for the southern hemisphere is mostly empty due to insufficient number of ground-based observations. The mean difference between GOME-2 and Brewer observations are within 5 DU for most of the years. However, we observed that there are years with positive bias while some years with negative bias. This is mostly related to the availability of ground-based data at different measurement sites. As some sites are bias high/low, and it will affect the statistic if they are not available for some years. On the other hand, the latitude dependent analysis shows that GOME-2 observations is consistently higher than the ground-based Brewer measurements in the Northern Hemisphere and result a positive bias of 2.3 to 3.5 DU on average.

3.3.2 Total column NO_2

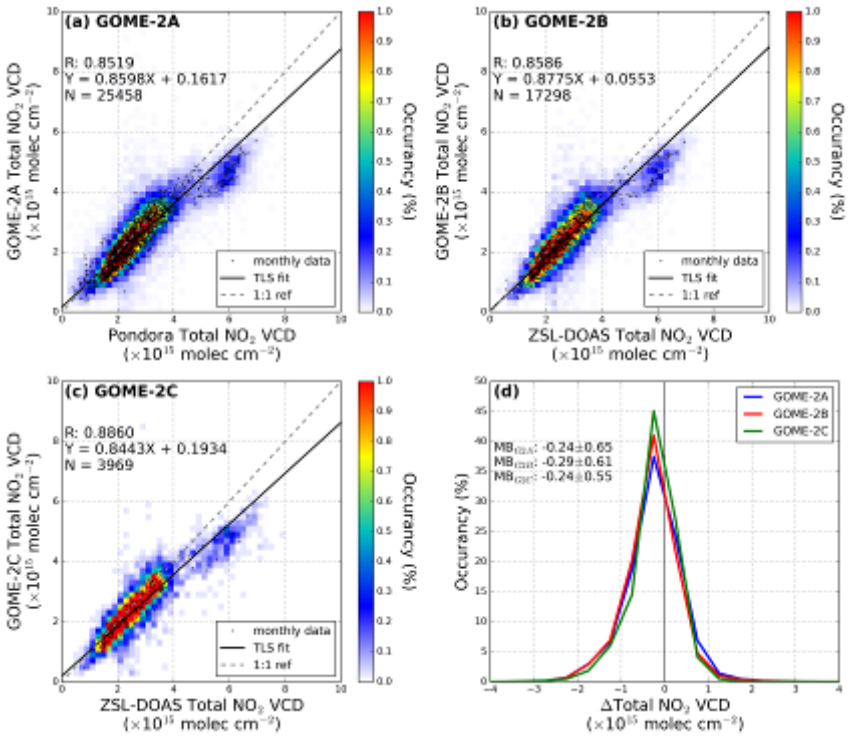

Figure 9. Comparison of daily and monthly total column NO_2 measured by the ground-based ZSL-DOAS to (a) GOME-2A, (b) GOME-2B and (c) GOME-2C. Histograms of the difference of total column NO_2 between GOME-2 and ZSL-DOAS observations are shown in (d).

Daily and monthly GOME-2 level 3 total column NO_2 are compared to the co-located ZSL-DOAS observations. Figure 9 shows the density scatter plots for the comparison of total column NO_2 between GOME-2 and ground-based ZSL-DOAS observations. Comparisons of GOME-2A, B & C data are shown in Figure 9a, b & c, respectively. Monthly data are also shown. Histograms of the differences between GOME-2 and ZSL-DOAS observations are shown in Figure 9d. Scatter plots show that GOME-2 monthly data is well in line with the daily data. GOME-2 level 3 total column NO_2 is in general in good agreement with ZSL-DOAS observations with Pearson correlation coefficient (R) of 0.85 to 0.88. However, GOME-2 observations are in general slightly lower than ZSL-DOAS observations. The slopes of the total least squares fit for the comparisons of all three instruments vary from 0.84 to 0.88 with offset ranging from 0.05 to 0.19×10^{15} molec cm^{-2}. Overall, the GOME-2 level 3 total NO_2 products are bias low by 0.24 to 0.29×10^{15} molec cm^{-2} compared to ground-based ZSL-DOAS measurements. Considering that the uncertainty of satellite and ground-based measurements is about 10%, the agreement between the two dataset is very satisfactory.

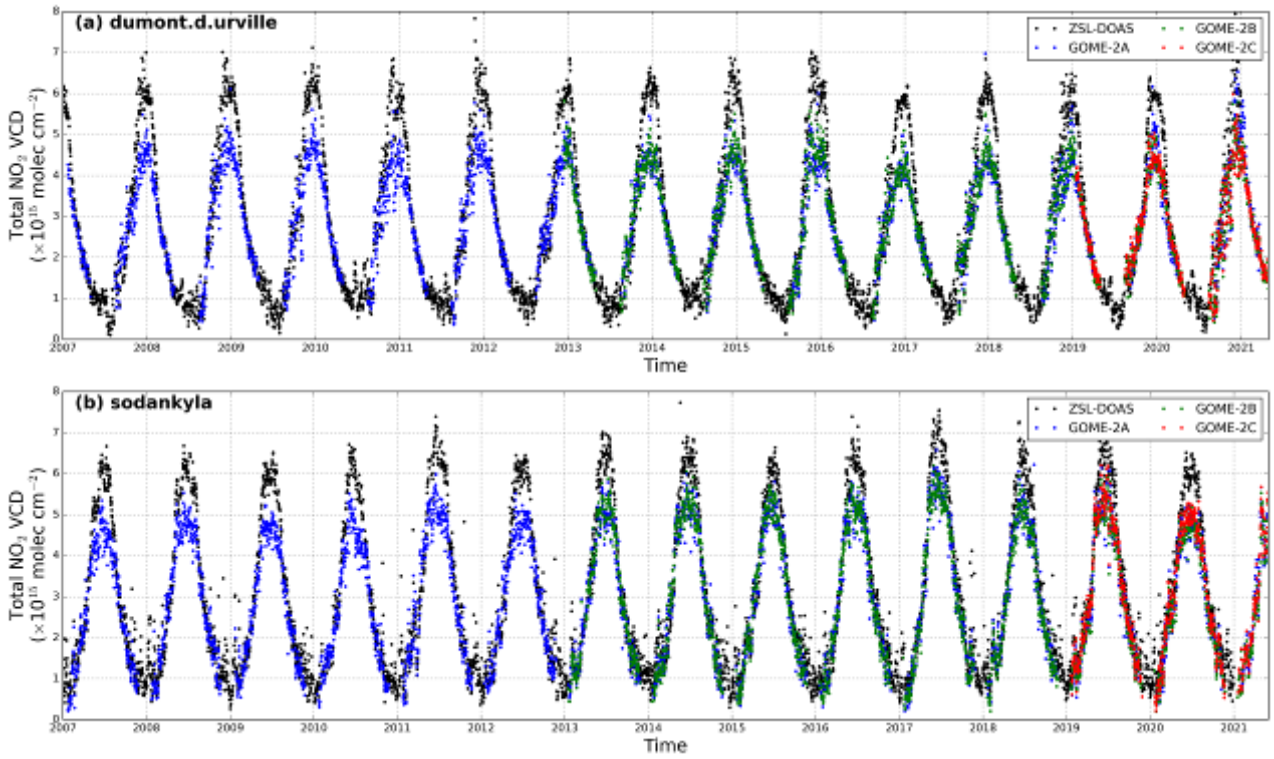

Figure 10: Time series of total column NO_2 measured by GOME-2A (blue), GOME-2B (green), GOME-2C (red) and ZSL-DOAS (black). Observations over (a) Dumont d'Urville, Antarctica and (b) Sodankylä, Finland are shown.

The scatter plots for all three instruments show a two clusters characteristic. The major cluster of total column NO_2 below 4×10^{15} molec cm^{-2} shows very good agreement between GOME-2 and ZSL-DOAS observations. The minor cluster at ~5-6$\times10^{15}$ molec cm^{-2} shows significant underestimation of NO_2 column by ~0.5-1.0$\times10^{15}$ molec cm^{-2} which is related to the measurement over Polar regions. Figure 10 shows the time series of total column NO_2 measured at Dumont d'Urville, Antarctica and Sodankylä, Finland. We observed that the total column NO_2 measured by GOME-2 is significantly lower than the ground-based ZSL-DOAS observations during summer months. This is because of the multiple overpasses over Polar Regions during summertime. Therefore, GOME-2 level 3 data represents the real "daily average" while ZSL-DOAS only capture the morning values. Due to the diurnal variation of NO_2, it is expected that ZSL-DOAS measurements in the morning is higher than the daily averages. If we do NOt consider these two stations in the analysis, the minor cluster in the scatter plots would be removed. In addition, the underestimation would reduce to 0.13 to 0.21$\times10^{15}$ molec cm^{-2}.

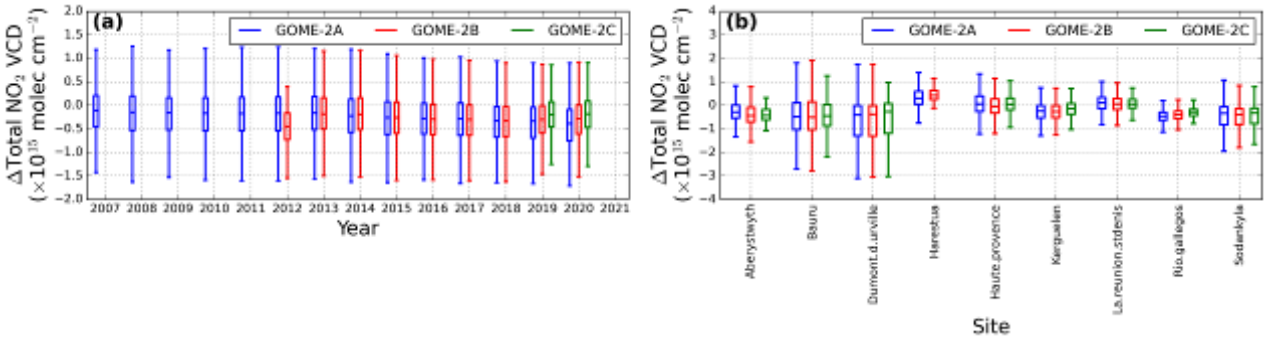

Figure 11. Comparison of total column NO_2 between ground-based ZSL-DOAS and GOME-2 observations. Data are sorted by year in (a), and measurement site in (b).

Figure 11 shows box plots of the statistic of the differences of total column NO_2 between GOME-2 level 3 product and co-located ZSL-DOAS measurements. Data are sorted by the measurement year (Figure 11a) and measurement site (Figure 11b). The mean differences between GOME-2 and ZSL-DOAS observations are within 0.3×10^{15} molec cm^{-2} for most of the years and this bias do not show significant temporal variation. Box plots for each measurement site show significant negative bias for some sites, i.e., Dumont d'Urville and Sodankylä. The reason of the negative bias has been explained above.

3.3.3 Tropospheric column NO_2

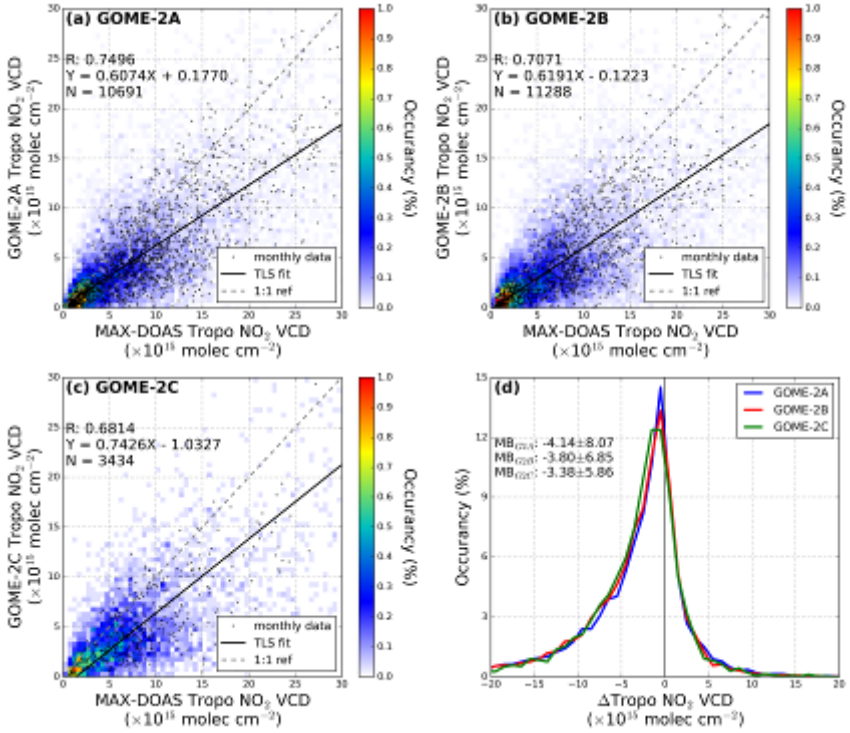

Figure 12. Comparison of daily and monthly tropospheric column NO_2 measured by the ground-based MAX-DOAS to (a) GOME-2A, (b) GOME-2B and (c) GOME-2C. Histograms of the difference of tropospheric column NO_2 between GOME-2 and MAX-DOAS observations are shown in (d).

Daily and monthly GOME-2 level 3 tropospheric column NO_2 are compared to the co-located MAX-DOAS observations. Figure 12 shows the density scatter plots for the comparison of tropospheric column NO_2 between GOME-2 and ground-based MAX-DOAS observations. Comparisons of GOME-2A, B & C data are shown in Figure 12a, b & c, respectively. Monthly data are also shown. Histograms of the differences between GOME-2 and MAX-DOAS observations are shown in Figure 12d. GOME-2 monthly tropospheric NO_2 data is consistent with the daily data, and daily data shows satisfactory correlation with ground-based MAX-DOAS observations with Pearson correlation coefficient (R) in a range of 0.68 to 0.75. However, GOME-2 tropospheric column NO_2 are in general ~30% lower than MAX-DOAS observations. The slopes of the total least squares fit for the comparisons of all three instruments vary from 0.61 to 0.74 with offset ranging from -1.03 to 0.18×10^{15} molec cm^{-2}. GOME-2 level 3 tropospheric NO_2 products on average show a negative bias of 3.38 to 4.14×10^{15} molec cm^{-2}. Considering that the sensitivity difference between satellite and ground-based MAX-DOAS measurements and the spatial averaging effect of large satellite footprint, the agreement between the two dataset is very satisfactory.

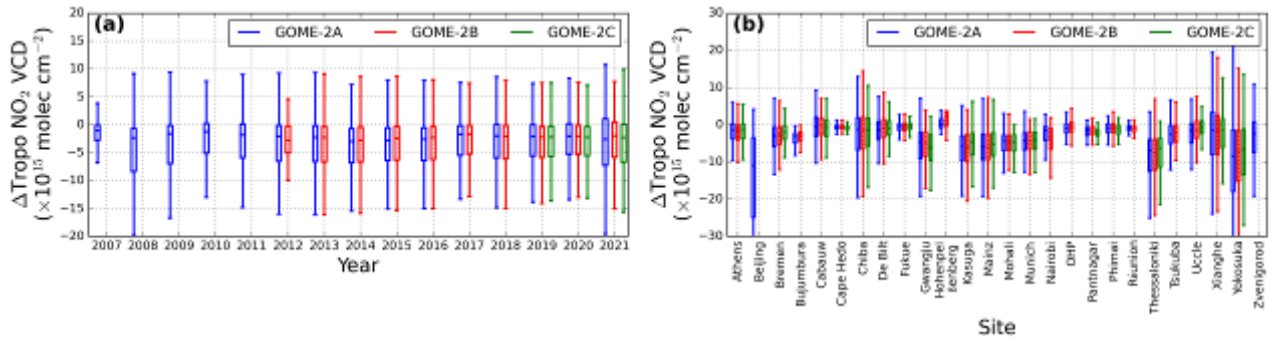

Figure 13. Comparison of tropospheric column NO_2 between ground-based MAX-DOAS and GOME-2 observations. Data are sorted by year in (a), and measurement site in (b).

Figure 13 shows box plots of the statistic of the differences of tropospheric column NO_2 between GOME-2 level 3 product and co-located MAX-DOAS measurements. Data is sorted by the measurement year (Figure 13a) and measurement site (Figure 13b). The mean differences between GOME-2 and MAX-DOAS observations are $\sim3\times10^{15}$ molec cm^{-2} for most of the years and this bias do not show significant temporal variation. Box plots for each measurement site show significant negative bias for some polluted sites, i.e., Beijing, China, Thessaloniki, Greece and Yokosuka, Japan. The reason of the negative bias has been explained above. The underestimation is significantly reduced over rural areas, e.g., Cape Hedo, Japan, Cabauw, Netherlands and Phimai, Thailand. These results are in line with the level 2 data that GOME-2 in general underestimates tropospheric column NO_2 over polluted areas.

3.3.4 Total column water vapour

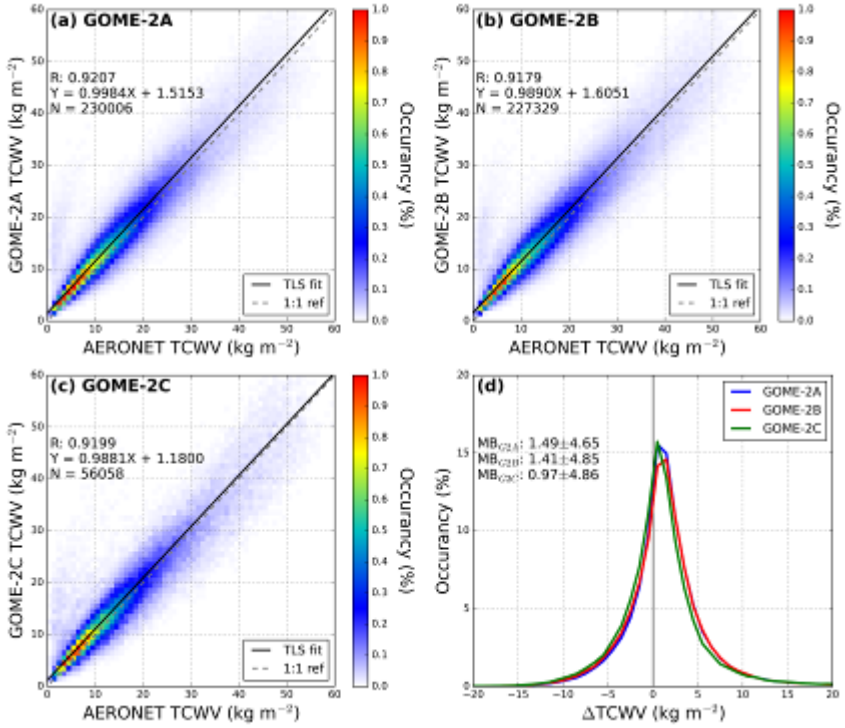

Figure 14. Comparison of daily total column water vapour measured by the ground-based sun-photometer to (a) GOME-2A, (b) GOME-2B and (c) GOME-2C. Histograms of the difference of total column water vapour between GOME-2 and sun-photometer observations are shown in (d).

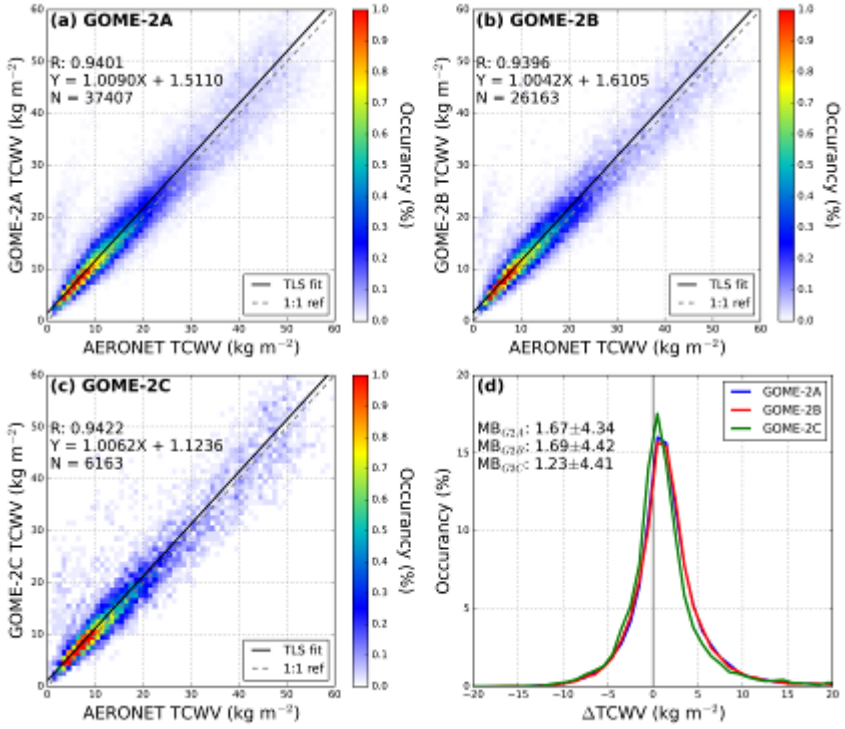

Figure 15. Comparison of monthly total column water vapour measured by the ground-based sun-photometer to (a) GOME-2A, (b) GOME-2B and (c) GOME-2C. Histograms of the difference of total column water vapour between GOME-2 and sun-photometer observations are shown in (d).

Daily GOME-2 level 3 total column water vapour are compared to the co-located sun-photometer observations. Figure 14 shows the density scatter plots for the comparison of total column water vapour column between GOME-2 and ground-based sun-photometer observations. Comparisons of GOME-2A, B & C data are shown in Figure 14a, b & c, respectively. Histograms of the differences between GOME-2 and MAX-DOAS observations are shown in Figure 14d. Similar plots for Monthly comparison are shown in Figure 15. GOME-2 monthly total column water vapour data is in general consistent with the daily data. GOME-2 daily observations are in good agreement with sun-photometer observations, with Pearson correlation coefficient (R) of ~0.92 for all three instruments. Monthly comparison shows higher correlation coefficient (R) of ~0.94. The slopes of least squares regression lines of daily comparison for all three GOME-2 sensors are very close to 1, while a small of 1.2 to 1.6 kg m^{-3} is observed. Monthly comparison shows similar characteristic with the slope of regression close to 1 and offset of 1.1-1.6 kg m^{-3}. GOME-2 level 3 total column water vapour in general show a positive bias of 1.0-1.7 kg m^{-3}. Considering that sun-photometer measurements are in general underestimating total column water vapour by 6-9% (Pérez-Ramírez et al., 2014) the positive bias of 1.0-1.7 kg m^{-3} is reasonable.

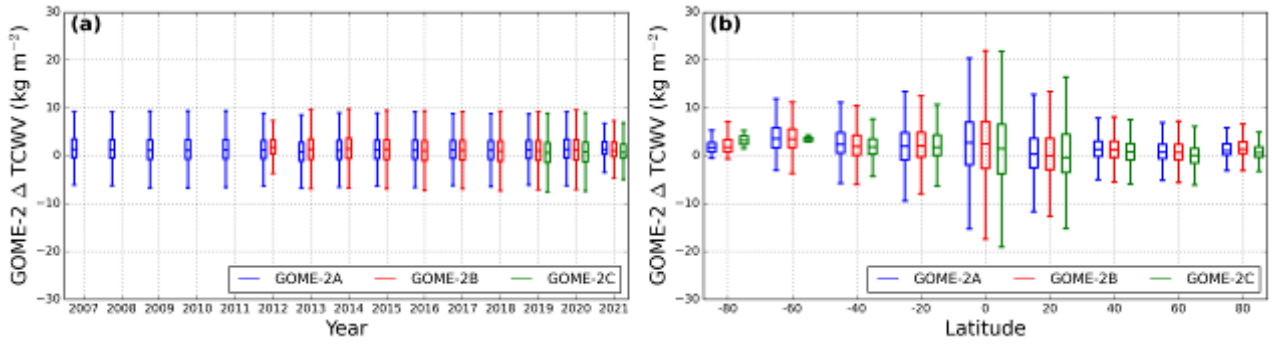

Figure 16. Comparison of total column water vapour between ground-based sun-photometer and GOME-2 observations. Data are sorted by year in (a), and latitude band in (b).

Figure 16 shows box plots of the statistic of the differences of total column water vapour between GOME-2 level 3 product and co-located sun-photometer measurements. Data is sorted by the measurement year (Figure 16a) and latitude band (Figure 16b). The bias between GOME-2 and sun-photometer observations is consistently at level of 1-2 kg m^{-3} throughout the entire measurement period. The latitude dependency analysis shows larger variations in the tropics, while the variations are much smaller at higher latitudes. The absolute differences for measurements over Polar Regions are slightly higher. This is mainly due to multiple overpasses over Polar Regions during summer months and result temporal mismatch.

3.3.5 Total column BrO

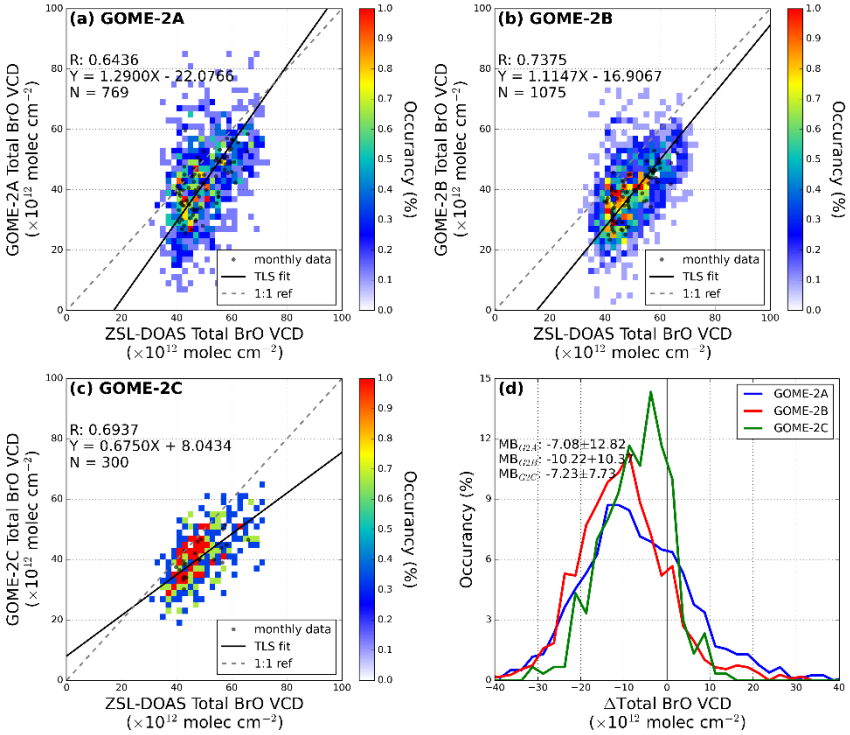

Figure 17. Comparison of daily and monthly total column BrO measured by the ground-based ZSL-DOAS at Harestua, Norway to (a) GOME-2A, (b) GOME-2B and (c) GOME-2C. Histograms of the difference of total column BrO between GOME-2 and MAX-DOAS observations are shown in (d).

Co-located daily and monthly GOME-2 level 3 total column BrO are compared to ZSL-DOAS observations at Harestua, Norway. Figure 17 shows the density scatter plots for the comparison of total column BrO between GOME-2 and ZSL-DOAS observations. Comparisons of GOME-2A, B & C data are shown in Figure 17a, b & c, respectively. Monthly data are also shown. Histograms of the differences between GOME-2 and ZSL-DOAS observations are shown in Figure 17d. We can see from the scatter plots that both GOME-2 and ZSL-DOAS BrO measurements are quite noisy, it is mainly due to the low absorption of BrO and thus low signal to noise ratio. Both daily and monthly GOME-2 level 3 data show quite good agreement with the ZSL-DOAS observations, with Pearson correlation coefficient (R) ranging from 0.64 to 0.74. In general, GOME-2 observations are underestimating BrO column by 7.0-10.2×10^{12} molec cm^{-2}.

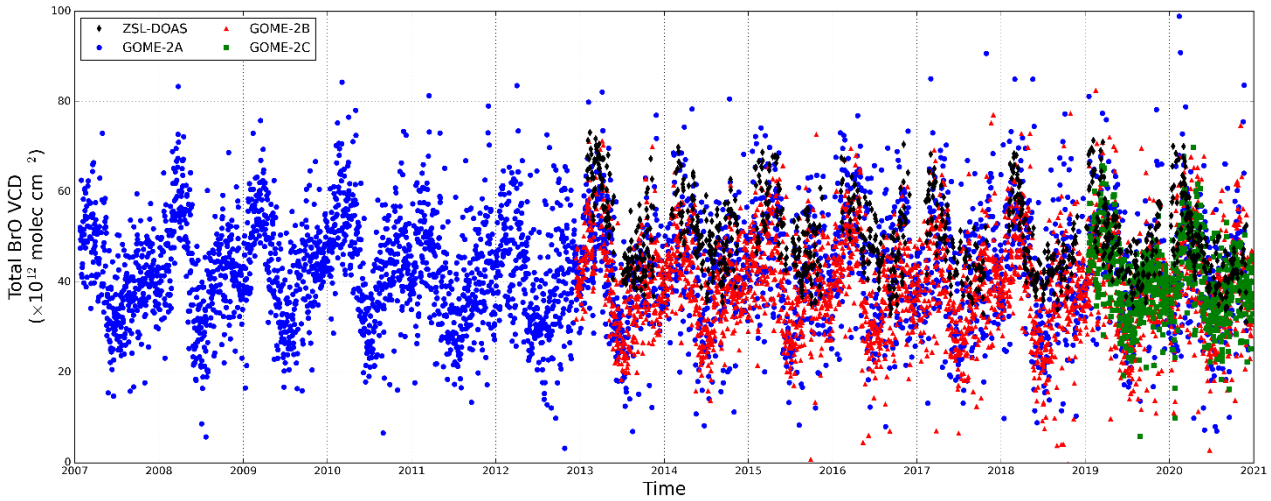

Figure 18: Time series of total column BrO measured by GOME-2A (blue), GOME-2B (green), GOME-2C (red) and ZSL-DOAS (black) at Harestua, Norway.

Figure 18 shows the time series of total column BrO measured at Harestua, Norway. Measurements from all three GOME-2 sensors show similar temporal variation trend with higher BrO level during summer and lower in winter which agrees with the ZSL-DOAS observations. However, GOME-2 observations are about 5-10×10^{12} molec cm^{-2} lower than the ZSL-DOAS data. This underestimation has also been reported in previous study (Theys et al. 2015). Considering that the ZSL-DOAS data have been empirically corrected for the offset caused by instrumental effect, the agreement between GOME-2 and ZSL-DOAS is deemed very satisfactory.

3.3.6 Total column formaldehyde

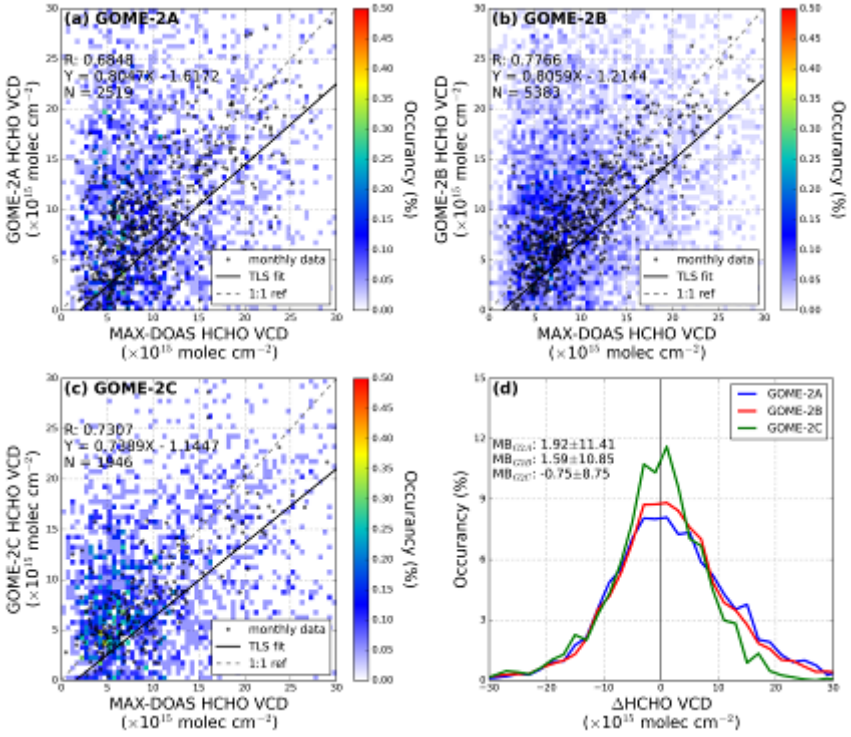

Figure 19. Comparison of daily and monthly total column HCHO measured by the ground-based MAX-DOAS to (a) GOME-2A, (b) GOME-2B and (c) GOME-2C. Histograms of the difference of total column HCHO between GOME-2 and MAX-DOAS observations are shown in (d).

Daily and monthly GOME-2 level 3 total column HCHO are compared to the co-located MAX-DOAS observations. Figure 19 shows the density scatter plots for the comparison of total column HCHO between GOME-2 and ground-based MAX-DOAS observations. Comparisons of GOME-2A, B & C data are shown in Figure 19a, b & c, respectively. Monthly data are also shown. Histograms of the differences between GOME-2 and MAX-DOAS observations are shown in Figure 19d. We can see from the scatter plots that both GOME-2 and MAX-DOAS HCHO measurements are quite noisy, it is mainly due to the low absorption of HCHO and thus low signal to noise ratio. However, when we look at the monthly averages, the GOME-2 level 3 data in general agrees with the ground-based MAX-DOAS observations. The Pearson correlation coefficient (R) between monthly GOME-2 and MAX-DOAS data ranges from 0.68 to 0.78. However, GOME-2 observations are in general underestimating total column HCHO by 20-25%. The slope of the total least squares regression line for the comparisons of all three instruments varies from 0.74 to 0.81 with offset ranging from -1.61 to -1.14×10^{15} molec cm^{-2}. GOME-2 level 3 total HCHO products on average show a small bias of -0.75 to 1.92×10^{15} molec cm^{-2} with standard deviation of 8.8 up to 11.4×10^{15} molec cm^{-2}. The underestimation is partly related to the a-prior profile used in GOME-2 retrieval and different of sensitivity between satellite and ground-based observations. The underestimation of level 3 product is in line with the level 2 product. Previous report (Theys et al. 2015) shows that the negative bias is significantly improved when MAX-DOAS profile is used for satellite column retrieval.

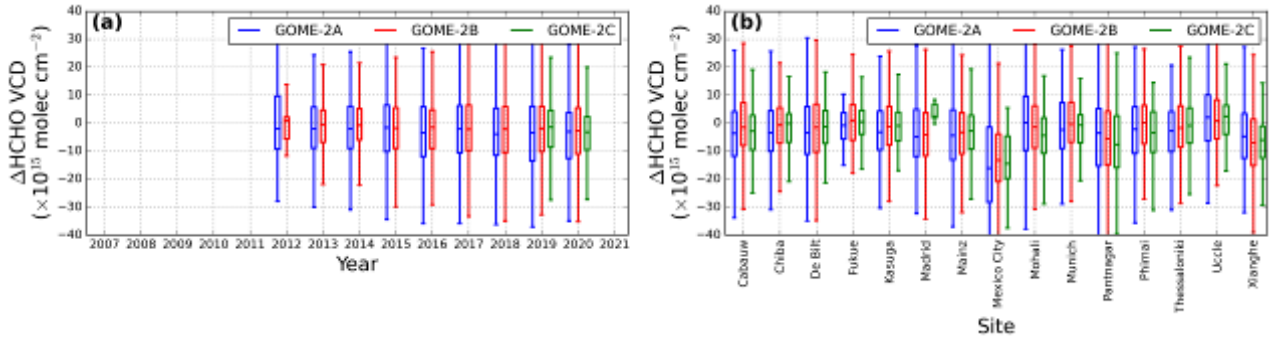

Figure 20. Comparison of total column HCHO between ground-based MAX-DOAS and GOME-2 observations. Data are sorted by year in (a), and measurement site in (b).

Figure 20 shows box plots of the statistic of the differences of total column HCHO between GOME-2 level 3 product and co-located MAX-DOAS measurements. Data is sorted by the measurement year (Figure 18a) and measurement site (Figure 18b). The mean differences between GOME-2 and MAX-DOAS observations are 1-2×10^{15} molec cm^{-2} for most of the years and do not show significant temporal variation. Box plots for each measurement site show that GOME-2 significantly underestimated HCHO column over polluted areas, i.e., Mexico City and Xianghe, China. The underestimation is related to the difference in sensitivity and this effect has been reported in previous level 2 validation studies (Pinardi et al. 2020).

3.3.7 Total column SO_2

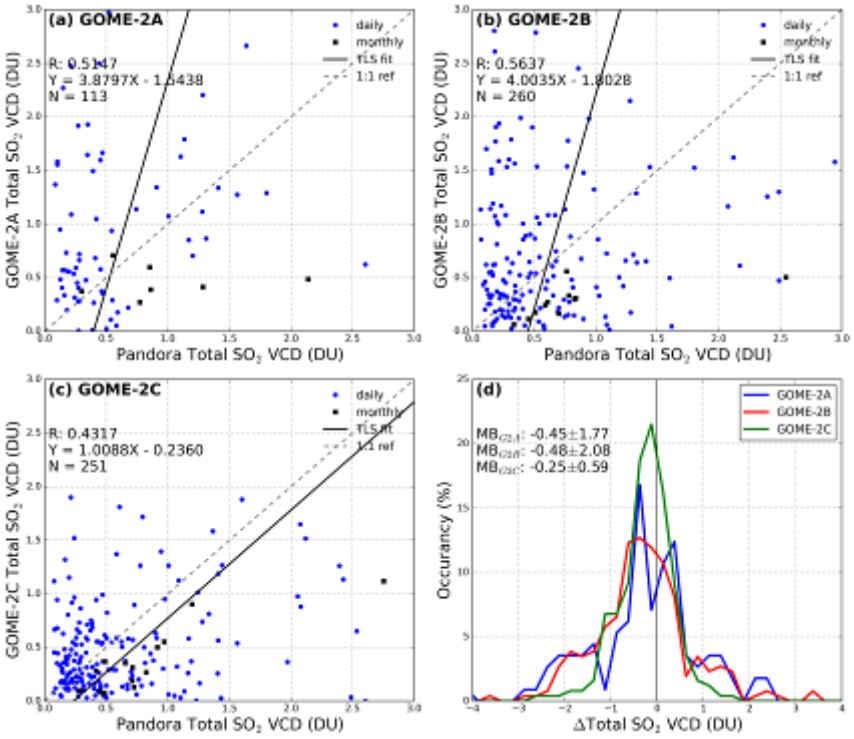

Figure 21. Comparison of daily and monthly total column SO_2 measured by Pandora instrument in Mexico City to (a) GOME-2A, (b) GOME-2B and (c) GOME-2C. Histograms of the difference of total column SO_2 between GOME-2 and Pandora observations are shown in (d).

Co-located daily and monthly GOME-2 level 3 total column SO_2 are compared to Pandora observations at Mexico City. Figure 21 shows the scatter plots for the comparison of total column SO_2 between GOME-2 and Pandora observations. Comparisons of GOME-2A, B & C data are shown in Figure 21a, b & c, respectively. Monthly data are also shown. Histograms of the differences between GOME-2 and Pandora observations are shown in Figure 20d. Due to the low absorption and abundancy of SO_2, both GOME-2 and Pandora measurements are quite noisy. Histogram shows that GOME-2 underestimated total column SO_2 by 0.25 to 0.48 DU.

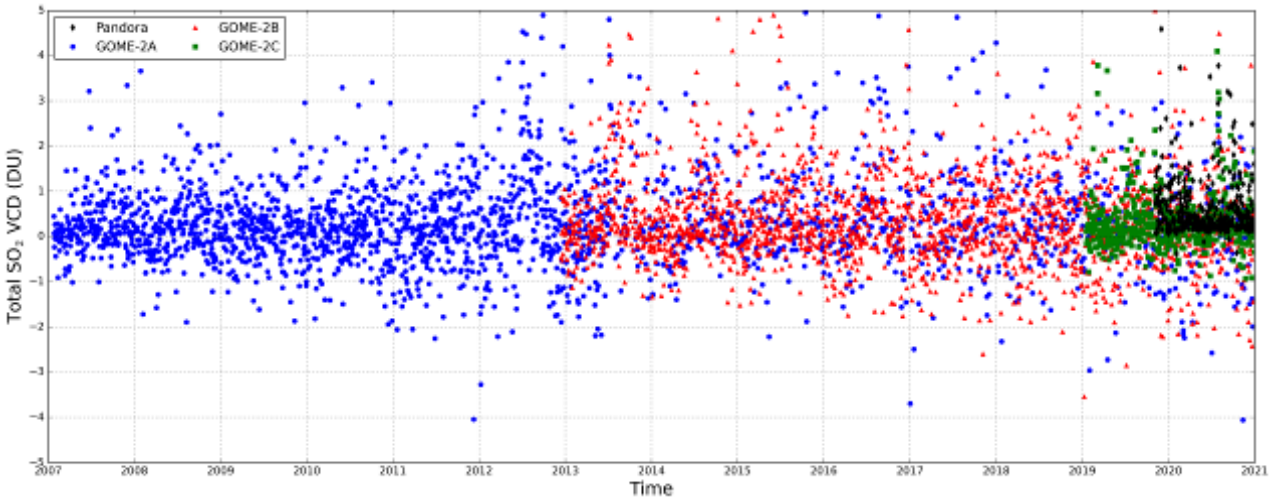

Figure 22: Time series of total column SO_2 measured by GOME-2A (blue), GOME-2B (green), GOME-2C (red) and Pandora (black) at Mexico City.

Figure 22 shows the time series of total column SO_2 measured at Mexico City. All three GOME-2 sensors show similar SO_2 columns. The overall averages are very close to zero and do not show any significant trend. Due to the low abundancy of SO_2 and low signal to noise ratio, there are considerable number of negative values. On the other hand, due to better signal to noise ratio, only very few negative values measured by Pandora. Considering the measurement noise of GOME-2, the agreement between GOME-2 and Pandora datasets is reasonable.

4. SUMMARY

In this report, the level 3 daily and monthly O_3, NO_2, water vapour, HCHO, BrO and SO_2 products of GOME-2A, GOME-2B and GOME-2C were verified and validated. As the GOME-2 level 3 products are produced based on the level 2 products, and the level 2 products have already been validated on regular bases. Therefore, this report focuses on the following issues.

1) Appropriate spatial resolution of level 3 products
2) Consistency between level 2 and 3 products
3) Consistency among three GOME-2 sensors
4) Comparison to ground-based observations

The spatial resolution of the level 3 product is examined by comparing maps gridded at various resolutions as well as the original level 2 data. The consistency among three GOME-2 sensors is investigated through time series of global averages, zonal averages, and bias. Finally, the accuracy of the level 3 products is validated through the comparison to ground-based observations.

We have re-sampled GOME-2 level 2 data onto various spatial resolutions, i.e., 0.1° × 0.1°, 0.25° × 0.25° and 0.5° × 0.5° and compared to the original level 2 data. All datasets show very similar spatial structures and the absolute values are consistency with the level 2 products. As expected, level 3 data sampled at higher spatial resolution (i.e., 0.1°) better preserve the original GOME-2 instrument footprint. However, lower resolution of 0.25° also preserves the spatial pattern of fast varying tropospheric species, i.e., NO_2, reasonably well. While a rather strong smoothing/averaging effect is observed from data gridded with lower spatial resolution (i.e., 0.5°). Therefore, we concluded that the spatial resolution of 0.25° is sufficient and appropriate for GOME-2 level 3 products.

The consistency of level 3 product among three GOME-2 sensors are investigated. Global average time series plots show that total column ozone and water vapour products from all GOME-2 sensors are consistent, with only a small bias of up to 3 DU (<1%) for ozone, and 0.9 kg m^{-2} (<5%) for water vapour. For total and tropospheric column NO_2 products, GOME-2A & B measurements are consistent with each other, while GOME-2C data show significant discrepancy compared to the other two sensors. This is mainly due to the instrumental issue of GOME-2C and therefore the spectral fitting band has to be changed to reduce the impact of this effect. In addition, the processer is also updated for GOME-2C (GDP 4.8 for GOME-2A & B and GDP 4.9 for GOME-2C). BrO observations from GOME-2B in general show a negative bias of ~1.0 - 1.5 × 10^{12} molec cm^{-2} compared to GOME-2A & C. GOME-2A HCHO columns are 1.5 - 1.9 × 10^{15} molec cm^{-2} lower than GOME-2B & C measurements. This is due to the underestimation over Amazon, Southeast Asia, and Australia. Total column SO_2 observations from GOME-2C are on average 0.5 DU lower than GOME-2A & B, resulting a slightly negative global average. Slightly higher global average of SO_2 measured by GOME-2A & B is related to the high values taken under extreme viewing geometry, i.e., high solar zenith angle.

For comparison of co-located GOME-2 measurements to ground-based observations, we found in general good agreement and the results are consistent with the level 2 validation studies.

Total column ozone:

Compare to Brewer observations

GOME-2A: Very good correlation with R of 0.96, small positive bias of 3.5±14.7 DU.

GOME-2B: Very good correlation with R of 0.96, small positive bias of 2.6±14.5 DU.

GOME-2C: Very good correlation with R of 0.97, small positive bias of 2.3±13.9 DU.

The bias between all three GOME-2 sensors and ground-based Brewer observations is below 1% which is within the uncertainty of Brewer measurements.

Total column NO_2:

Compare to ZSL-DOAS observations

GOME-2A: Very good correlation with R of 0.85, small negative bias of $-0.24\pm0.65\times10^{15}$ molec cm^{-2}.

GOME-2B: Very good correlation with R of 0.86, small negative bias of $-0.29\pm0.61\times10^{15}$ molec cm^{-2}.

GOME-2C: Very good correlation with R of 0.89, small negative bias of $-0.24\pm0.55\times10^{15}$ molec cm^{-2}.

The negative bias is in relation to temporal mismatch of measurements over Polar Regions. Considering that the uncertainty of satellite and ground-based measurements is about 10%, the agreement between the GOME-2 and ground-based is very satisfactory.

Tropospheric column NO_2:

Compare to MAX-DOAS observations

GOME-2A: Good correlation with R of 0.75, negative bias of $-4.1\pm8.1\times10^{15}$ molec cm^{-2}.

GOME-2B: Good correlation with R of 0.71, negative bias of $-3.8\pm6.9\times10^{15}$ molec cm^{-2}.

GOME-2C: Good correlation with R of 0.68, negative bias of $-3.4\pm5.9\times10^{15}$ molec cm^{-2}.

Discrepancy is due to the difference in sensitivity between satellite and ground-based measurements and the spatial averaging effect of large satellite footprint. Considering these factors, the agreement between GOME-2 and ground-based dataset is very satisfactory.

Total column water vapour:

Compare to sun-photometer observations

GOME-2A: Very good correlation with R of 0.92, small positive bias of 1.5±4.7 kg m^{-2}.

GOME-2B: Very good correlation with R of 0.92, small positive bias of 1.4±4.9 kg m^{-2}.

GOME-2C: Very good correlation with R of 0.92, small positive bias of 1.0±4.9 kg m^{-2}.

Considering that sun-photometer measurements are in general underestimating total column water vapour by 6-9% the small positive bias is very satisfactory.

Total column BrO:

Compare to ZSL-DOAS observations at Harestua, Norway

GOME-2A: Good correlation with R of 0.64, small bias of $7.1\pm12.8\times10^{12}$ molec cm^{-2}.

GOME-2B: Good correlation with R of 0.74, small bias of $10.2\pm10.4\times10^{12}$ molec cm^{-2}.

GOME-2C: Good correlation with R of 0.69, small bias of $7.2\pm7.7\times10^{12}$ molec cm^{-2}.

Considering that the ZSL-DOAS data have been empirically corrected for the offset caused by instrumental effect, the agreement between GOME-2 and ZSL-DOAS is deemed satisfactory.

Total column HCHO:

Compare to MAX-DOAS observations

GOME-2A: Good correlation with R of 0.68, bias of $1.9\pm11.4\times10^{15}$ molec cm^{-2}.

GOME-2B: Good correlation with R of 0.78, bias of $1.6\pm10.9\times10^{15}$ molec cm^{-2}.

GOME-2C: Good correlation with R of 0.73, bias of $-0.8\pm8.8\times10^{15}$ molec cm^{-2}.

Considering the low signal to noise ratio of HCHO measurements, the agreement between GOME-2 and Pandora datasets is reasonable.

Total column SO_2:

Compare to Pandora observations at Mexico City

GOME-2A: Reasonable correlation with R of 0.51, small negative bias of 0.45±1.8 DU.

GOME-2B: Reasonable correlation with R of 0.56, small negative bias of 0.48±2.1 DU.

GOME-2C: Reasonable correlation with R of 0.43, small negative bias of 0.25±0.6 DU.

Considering the low signal to noise ratio of SO_2 measurements, the agreement between GOME-2 and Pandora datasets is reasonable.

From the above, we conclude that the daily and monthly GOME-2 level 3 products of O_3, NO_2, water vapour, BrO, HCHO and SO_2 for GOME2A, GOME2B and GOME2C fulfil the product requirements and are fit for public release.

REFERENCES

Alexandrov, M.D., Schmid, B., Turner, D.D., Cairns, B., Oinas, V., Lacis, A.A., Gutman, S.I., Westwater, E.R., Smirnov, A., Eilers, J.. Columnar water vapor retrievals from multifilter rotating shadowband radiometer data. Journal of Geophysical Research: Atmospheres 2009;114(D2). doi:10.1029/2008JD010543.

Antón, M., Loyola, D., López, M., Vilaplana, J.M., Bañón, M., Zimmer, W., Serrano, A.. Comparison of GOME-2/MetOp total ozone data with brewer spectroradiometer data over the Iberian Peninsula. Annales Geophysicae 2009;27(4):1377–1386. doi:10.5194/angeo-27-1377-2009.

Balis, D., Kroon, M., Koukouli, M.E., Brinksma, E.J., Labow, G., Veefkind, J.P., McPeters, R.D.. Validation of Ozone Monitoring Instrument total ozone column measurements using brewer and dobson spectrophotometer ground-based observations. Journal of Geophysical Research: Atmospheres 2007a;112(D24). doi:10.1029/2007JD008796.

Balis, D., Lambert, J.C., Van Roozendael, M., Spurr, R., Loyola, D., Livschitz, Y., Valks, P., Amiridis, V., Gerard, P., Granville, J., Zehner, C.. Ten years of GOME/ERS2 total ozone data—the new GOME data processor (GDP) version 4: 2. ground-based validation and comparisons with TOMS v7/v8. Journal of Geophysical Research: Atmospheres 2007b;112(D7). doi:10.1029/2005JD006376.

Brinksma, E.J., Pinardi, G., Volten, H., Braak, R., Richter, A., Schönhardt, A., van Roozendael, M., Fayt, C., Hermans, C., Dirksen, R.J., Vlemmix, T., Berkhout, A.J.C., Swart, D.P.J., Oetjen, H., Wittrock, F., Wagner, T., Ibrahim, O.W., de Leeuw, G., Moerman, M., Curier, R.L., Celarier, E.A., Cede, A., Knap, W.H., Veefkind, J.P., Eskes, H.J., Allaart, M., Rothe, R., Piters, A.J.M., Levelt, P.F.. The 2005 and 2006 DANDELIONS NO_2 and aerosol intercomparison campaigns. Journal of Geophysical Research: Atmospheres 2008;113(D16). doi:10.1029/2007JD008808.

Celarier, E.A., Brinksma, E.J., Gleason, J.F., Veefkind, J.P., Cede, A., Herman, J.R., Ionov, D., Goutail, F., Pommereau, J.P., Lambert, J.C., van Roozendael, M., Pinardi, G., Wittrock, F., Schönhardt, A., Richter, A., Ibrahim, O.W., Wagner, T., Bojkov, B., Mount, G., Spinei, E., Chen, C.M., Pongetti, T.J., Sander, S.P., Bucsela, E.J., Wenig, M.O., Swart, D.P.J., Volten, H., Kroon, M., Levelt, P.F.. Validation of Ozone Monitoring Instrument nitrogen dioxide columns. Journal of Geophysical Research: Atmospheres 2008;113(D15). doi:10.1029/2007JD008908.

Chan, K., Wiegner, M., Wenig, M., Pöhler, D.. Observations of tropospheric aerosols and NO_2 in Hong Kong over 5years using ground based MAX-DOAS. Science of The Total Environment 2018;619-620:1545–1556. doi:10.1016/j.scitotenv.2017.10.153.

Chan, K.L., Wang, Z., Ding, A., Heue, K.P., Shen, Y., Wang, J., Zhang, F., Shi, Y., Hao, N., Wenig, M.. MAX-DOAS measurements of tropospheric NO_2 and HCHO in Nanjing and a comparison to ozone monitoring instrument observations. Atmospheric Chemistry and Physics 2019;19(15):10051–10071. doi:10.5194/acp-19-10051-2019.

Chan, K.L., Wiegner, M., van Geffen, J., De Smedt, I., Alberti, C., Cheng, Z., Ye, S., Wenig, M..MAX-DOAS measurements of tropospheric NO_2 and HCHO in Munich and the comparison to OMI and TROPOMI satellite observations. Atmospheric Measurement Techniques 2020;13(8):4499–4520. doi:10.5194/amt-13-4499-2020.

Compernolle, S., Verhoelst, T., Pinardi, G., Granville, J., Hubert, D., Keppens, A., Niemeijer, S., Rino, B., Bais, A., Beirle, S., Boersma, F., Burrows, J.P., De Smedt, I., Eskes, H., Goutail, F., Hendrick, F., Lorente, A., Pazmino, A., Piters, A., Peters, E., Pommereau, J.P., Remmers, J.,

Richter, A., van Geffen, J., Van Roozendael, M., Wagner, T., Lambert, J.C.. Validation of Aura-OMI QA4ECV NO_2 climate data records with ground-based DOAS networks: the role of measurement and comparison uncertainties. tropospheric Chemistry and Physics 2020;20(13):8017–8045. doi:10.5194/acp-20-8017-2020.

De Smedt, I., Pinardi, G., Vigouroux, C., Compernolle, S., Bais, A., Benavent, N., Boersma, F., Chan, K.L., Donner, S., Eichmann, K.U., Hedelt, P., Hendrick, F., Irie, H., Kumar, V., Lambert, J.C., Langerock, B., Lerot, C., Liu, C., Loyola, D., Piters, A., Richter, A., Rivera Cárdenas, C., Romahn, F., Ryan, R.G., Sinha, V., Theys, N., Vlietinck, J., Wagner, T., Wang, T., Yu, H., Van Roozendael, M.. Comparative assessment of TROPOMI and OMI formaldehyde observations and validation against MAX-DOAS network column measurements. Atmospheric Chemistry and Physics 2021;21(16):12561–12593. doi:10.5194/acp-21-12561-2021.

Drosoglou, T., Bais, A.F., Zyrichidou, I., Kouremeti, N., Poupkou, A., Liora, N., Giannaros, C., Koukouli, M.E., Balis, D., Melas, D.. Comparisons of ground-based tropospheric NO_2 MAX-DOAS measurements to satellite observations with the aid of an air quality model over the Thessaloniki area, Greece. Atmospheric Chemistry and Physics 2017;17(9):5829–5849. doi:10.5194/acp-17-5829-2017.

Garane, K., Koukouli, M.E., Verhoelst, T., Lerot, C., Heue, K.P., Fioletov, V., Balis, D., Bais, A., Bazureau, A., Dehn, A., Goutail, F., Granville, J., Griffin, D., Hubert, D., Keppens, A., Lambert, J.C., Loyola, D., McLinden, C., Pazmino, A., Pommereau, J.P., Redondas, A., Romahn, F., Valks, P., Van Roozendael, M., Xu, J., Zehner, C., Zerefos, C., Zimmer, W.. TROPOMI/S5P total ozone column data: global ground-based validation and consistency with other satellite missions. Atmospheric Measurement Techniques 2019;12(10):5263–5287. doi:10.5194/amt-12-5263-2019.

Garane, K., Lerot, C., Coldewey-Egbers, M., Verhoelst, T., Koukouli, M.E., Zyrichidou, I., Balis, D.S., Danckaert, T., Goutail, F., Granville, J., Hubert, D., Keppens, A., Lambert, J.C., Loyola, D., Pommereau, J.P., Van Roozendael, M., Zehner, C.. Quality assessment of the ozone cci climate research data package (release 2017) – part 1: Ground-based validation of total ozone column data products. Atmospheric Measurement Techniques 2018;11(3):1385–1402. doi:10.5194/amt-11-1385-2018.

Hendrick, F., Van Roozendael, M., Chipperfield, M.P., Dorf, M., Goutail, F., Yang, X., Fayt, C., Hermans, C., Pfeilsticker, K., Pommereau, J.P., Pyle, J.A., Theys, N., De Mazière, M.. Retrieval of stratospheric and tropospheric BrO profiles and columns using ground-based zenith-sky DOAS observations at Harestua, 60◦ n. Atmospheric Chemistry and Physics 2007;7(18):4869–4885. doi:10.5194/acp-7-4869-2007.

Holben, B., Eck, T., Slutsker, I., Tanré, D., Buis, J., Setzer, A., Vermote, E., Reagan, J., Kaufman, Y., Nakajima, T., Lavenu, F., Jankowiak, I., Smirnov, A.. AERONET—a federated instrument network and data archive for aerosol characterization. Remote Sensing of Environment 1998;66(1):1–16. doi:10.1016/S0034-4257(98)00031-5.

Holben, B.N., Tanré, D., Smirnov, A., Eck, T.F., Slutsker, I., Abuhassan, N., Newcomb, W.W., Schafer, J.S., Chatenet, B., Lavenu, F., Kaufman, Y.J., Castle, J.V., Setzer, A., Markham, B., Clark, D., Frouin, R., Halthore, R., Karneli, A., O'Neill, N.T., Pietras, C., Pinker, R.T., Voss, K., Zibordi, G.. An emerging ground-based aerosol climatology: Aerosol optical depth from AERONET. Journal of Geophysical Research: Atmospheres 2001;106(D11):12067–12097. doi:10.1029/2001JD900014.

Ionov, D.V., Timofeyev, Y.M., Sinyakov, V.P., Semenov, V.K., Goutail, F., Pommereau, J.P., Bucsela, E.J., Celarier, E.A., Kroon, M.. Ground-based validation of EOS-Aura OMI NO_2 vertical column data in the midlatitude mountain ranges of Tien Shan (Kyrgyzstan) and Alps (France). Journal of Geophysical Research: Atmospheres 2008;113(D15). doi:10.1029/2007JD008659.

Irie, H., Kanaya, Y., Akimoto, H., Tanimoto, H., Wang, Z., Gleason, J.F., Bucsela, E.J.. Validation of OMI tropospheric NO_2 column data using MAX-DOAS measurements deep inside the North China Plain in June 2006: Mount Tai experiment 2006. Atmospheric Chemistry and Physics 2008;8(22):6577–6586. doi:10. 5194/acp-8-6577-2008.

Kanaya, Y., Irie, H., Takashima, H., Iwabuchi, H., Akimoto, H., Sudo, K., Gu, M., Chong, J., Kim, Y.J., Lee, H., Li, A., Si, F., Xu, J., Xie, P.H., Liu, W.Q., Dzhola, A., Postylyakov, O., Ivanov, V., Grechko, E., Terpugova, S., Panchenko, M.. Long-term max-doas network observations of NO_2 in Russia and Asia (MADRAS) during the period 2007–2012: instrumentation, elucidation of climatology, and comparisons with OMI satellite observations and global model simulations. Atmospheric Chemistry and Physics 2014;14(15):7909–7927. doi:10.5194/acp-14-7909-2014.

Kerr, J.B., Asbridge, I.A., Evans, W.F.J.. Intercomparison of total ozone measured by the Brewer and Dobson spectrophotometers at Toronto. Journal of Geophysical Research: Atmospheres 1988;93(D9):11129–11140. doi:10.1029/JD093iD09p11129.

Koukouli, M.E., Balis, D.S., Loyola, D., Valks, P., Zimmer, W., Hao, N., Lambert, J.C., Van Roozendael, M., Lerot, C., Spurr, R.J.D.. Geophysical validation and long-term consistency between GOME-2/MetOp-A total ozone column and measurements from the sensors GOME/ERS-2, SCIAMACHY/ENVISAT and OMI/Aura. Atmospheric Measurement Techniques 2012;5(9):2169–2181. doi:10.5194/amt-5-2169-2012.

Koukouli, M.E., Lerot, C., Granville, J., Goutail, F., Lambert, J.C., Pommereau, J.P., Balis, D., Zyrichidou, I., Van Roozendael, M., Coldewey-Egbers, M., Loyola, D., Labow, G., Frith, S., Spurr, R., Zehner, C.. Evaluating a new homogeneous total ozone climate data record from GOME/ERS-2, SCIAMACHY/Envisat, and GOME-2/MetOp-A. Journal of Geophysical Research: Atmospheres 2015;120(23):12,296–12,312. doi:10.1002/2015JD023699.

Kumar, V., Beirle, S., Dörner, S., Mishra, A.K., Donner, S., Wang, Y., Sinha, V., Wagner, T.. Long-term MAX-DOAS measurements of NO_2, HCHO, and aerosols and evaluation of corresponding satellite data products over Mohali in the Indo-Gangetic plain. Atmospheric Chemistry and Physics 2020;20(22):14183–14235. doi:10.5194/acp-20-14183-2020.

Li, X., Brauers, T., Hofzumahaus, A., Lu, K., Li, Y.P., Shao, M., Wagner, T., Wahner, A.. MAX-DOAS measurements of NO_2 , HCHO and CHOCHO at a rural site in southern china. Atmospheric Chemistry and Physics 2013;13(4):2133–2151. doi:10.5194/acp-13-2133-2013.

Loyola, D.G., Koukouli, M.E., Valks, P., Balis, D.S., Hao, N., Van Roozendael, M., Spurr, R.J.D., Zimmer, W., Kiemle, S., Lerot, C., Lambert, J.C.. The GOME-2 total column ozone product: Retrieval algorithm and ground-based validation. Journal of Geophysical Research: Atmospheres 2011;116(D7). doi:10.1029/2010JD014675.

Ma, J.Z., Beirle, S., Jin, J.L., Shaiganfar, R., Yan, P., Wagner, T.. Tropospheric NO_2 vertical column densities over beijing: results of the first three years of ground-based MAX-DOAS measurements (2008–2011) and satellite validation. Atmospheric Chemistry and Physics 2013;13(3):1547–1567. doi:10.5194/acp-13-1547-2013.

Merlaud, A., Theys, N., Hendrick, F., Van Gent, J., Pinardi, G., Van Roozendael, M., Chan, K. L., Heue, K.-P. and Valks, P., AC-SAF ORR Validation Report for GOME-2C Total BrO, SAF/AC/IASB/VR/BRO, 2020, Issue, 1/1, https://acsaf.org/docs/vr/Validation_Report_OTO_BrO_May_2020.pdf

Munro, R., Lang, R., Klaes, D., Poli, G., Retscher, C., Lindstrot, R., Huckle, R., Lacan, A., Grzegorski, M., Holdak, A., Kokhanovsky, A., Livschitz, J., Eisinger, M.. The GOME-2 instrument on the metop series of satellites: instrument design, calibration, and level 1 data processing – an overview. Atmospheric Measurement Techniques 2016;9(3):1279–1301. doi:10.5194/amt-9-1279-2016.

Pérez-Ramírez, D., Whiteman, D.N., Smirnov, A., Lyamani, H., Holben, B.N., Pinker, R., Andrade, M., Alados-Arboledas, L.. Evaluation of AERONET precipitable water vapor versus microwave radiometry, GPS, and radiosondes at ARM sites. Journal of Geophysical Research: Atmospheres 2014;119(15):9596–9613. doi:10.1002/2014JD021730.

Pinardi, G., Yu, H., Van Roozendael, M., Van Gent, J., Chan, K. L. and Valks, P., AC-SAF ORR Validation Report for GOME-2C Total HCHO, 2020, SAF/AC/IASB/VR/HCHO, Issue, 1/2, https://acsaf.org/docs/vr/Validation_Report_NTO_OTO_HCHO_May_2020.pdf

Takashima, H., Kanaya, Y., Irie, H.. Spatiotemporal inhomogeneity in NO_2 over Fukuoka observed by ground-based MAX-DOAS. Atmospheric Environment 2015;100:117–123. doi:10.1016/j.atmosenv.2014.10.057.

Theys, N., Hendrick, F., Van Gent, J., Van Roozendael, M., Hao, N., Valks, P., O_3M SAF Validation Report for GOME-2A & B Total BrO, 2015, SAF/O3M/BIRA/VR/BRO, Issue, 1/1, https://acsaf.org/docs/vr/Validation_Report_OTO_DR_BrO_GDP48_Dec_2015.pdf

Vigouroux, C., Hendrick, F., Stavrakou, T., Dils, B., De Smedt, I., Hermans, C., Merlaud, A., Scolas, F., Senten, C., Vanhaelewyn, G., Fally, S., Carleer, M., Metzger, J.M., Müller, J.F., Van Roozendael, M., De Mazière, M.. Ground-based FTIR and MAX-DOAS observations of formaldehyde at réunion island and comparisons with satellite and model data. Atmospheric Chemistry and Physics 2009;9(24):9523–9544. doi:10.5194/acp-9-9523-2009.